

THE DYNAMIC ANALYSIS OF CONTACT SEPARATION
DUE TO IMPACT IN A CONTINUOUS,
REDUNDANT CONTACT SYSTEM

By

HEINZ WALTER SCHMITT

Bachelor of Mechanical Engineering
Brooklyn Polytechnic Institute
New York, New York
1960


Master of Science
University of New Mexico
Albuquerque, New Mexico
1962

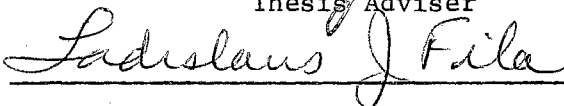
Submitted to the faculty of the Graduate College of
the Oklahoma State University
in partial fulfillment of the requirements
for the degree of
DOCTOR OF PHILOSOPHY
May, 1966

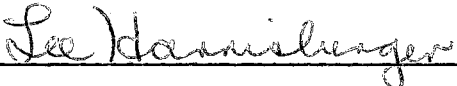
OKLAHOMA
STATE UNIVERSITY
LIBRARY
NOV 10 1966

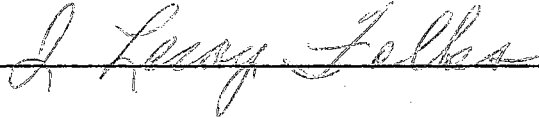
THE DYNAMIC ANALYSIS OF CONTACT SEPARATION
DUE TO IMPACT IN A CONTINUOUS,
REDUNDANT CONTACT SYSTEM

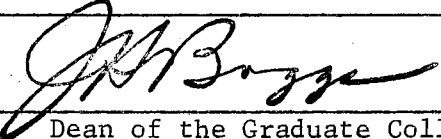
Thesis Approved:



Thesis Adviser








Dean of the Graduate College

621804

ACKNOWLEDGMENTS

I wish to thank Sandia Corporation of Albuquerque, New Mexico, for sponsoring the research program at Oklahoma State University which precipitated this work and for supplying both equipment and experimental units. The consultation and cooperation of Mr. J. W. Gear, Jr. of Sandia Corporation is greatly appreciated.

Particular thanks is offered to Dr. R. L. Lowery, research project director and thesis adviser, for his aid and encouragement during the course of this research. In addition, the efforts of Professor L. J. Fila, Dr. Lee Harrisberger, and Dr. J. L. Folks, committee members, are appreciated. The cooperation of the staff of the Mechanical Engineering Laboratory is also recognized.

I am forever indebted to my wife, Barbara, for her continued encouragement, understanding, and her numerous sacrifices, without which this undertaking would not have reached fruition.

Mr. N. N. Reddy is thanked for his general assistance in this research. Mr. E. Hardy is thanked for his help with the drafting work. Mrs. Betty Stewart is thanked for the typing of the final manuscript.

TABLE OF CONTENTS

Chapter	Page
I. INTRODUCTION	1
Definition of Problem	2
II. PREVIOUS WORK.	4
III. MATHEMATICAL MODEL	13
Transverse Vibrational Response of Upper Contact Spring.	13
Transmission of the Impulse by the Contact Separator.	18
Transverse Vibrational Response of Lower Contact.	21
Derivation of the Impulse Expression.	23
IV. ANALYSIS AND DISCUSSION OF THE EQUATIONS CONSTITUTING THE MATHEMATICAL MODEL	27
Governing Equation.	28
Coefficient of Restitution and Initial Deflection	31
Normal Mode Function.	32
Mass Ratio.	39
V. EXPERIMENTAL MODEL AND INSTRUMENTATION	43
Description of the Model.	43
Instrumentation	46
VI. EXPERIMENTAL PROCEDURE AND RESULTS	51
Model Parameters.	51
Coefficient of Restitution.	63
Test Procedure.	67
VII. CONCLUSIONS AND RECOMMENDATIONS.	73
Recommendations for Future Analysis	74
BIBLIOGRAPHY	76

Chapter	Page
APPENDICES.	80
A. Response of a Cantilever Beam to Initial Displacement Start.	80
B. Response of a Cantilever Beam to an Impulse at its Free End.	84
C. Response of a Clamped-Clamped Beam to an Impulse at Mid-Span	88
D. Response of a Cantilever Beam to an Initial Velocity Start at its Free End.	91
E. Displacement Equations for Repeated Impacts of a Cantilever Beam, at its Free End, With a Rigid Body	94
F. List of Major Instrumentation.	98
G. Fortran Program for the Lower Contact Displacement	99

LIST OF TABLES

Table	Page
I. Theoretical and Experimental Contact Natural Frequencies.	59
II. Theoretical and Experimental Contact Separator Natural Frequency.	61
III. Equivalent Length of the Contact Separators.	62

LIST OF FIGURES

Figure	Page
1. Contact Spring System	2
2. Theoretical Model	14
3. Impulse to the Contact Separator.	19
4. Initial Velocity Start to a Cantilever Beam	21
5. Theoretical Values of the Maximum Contact Displacement Versus Contact Separator Thickness.	33
6. Maximum Contact Displacement Versus x_3/L_3	35
7. Contact Displacement Versus Time.	38
8. Maximum Contact Displacement Versus Mass Ratio.	41
9. Experimental Model.	44
10. Solenoid and Contact Separator Clamping Arrangement	45
11. Photocell and Light Source Arrangement.	47
12. Block Diagram of the Instrumentation.	49
13. Experimental Model With Instrumentation	50
14. Velocity Transducer Calibration Arrangement	52
15. Experimental Arrangement for Finding the Natural Frequencies of the Contacts	55
16. Sand Pattern for the Second Mode of the Contact	56
17. Sand Pattern for the Third Mode of the Contact.	57
18. Sand Pattern for the Fourth Mode of the Contact	58
19. Velocity Transducer Response.	64
20. Coefficient of Restitution Parameters	65

Figure	Page
21. Corrected Theoretical Maximum Contact Displacement Versus Contact Separator Thickness	68
22. Contact Displacement Response.	69
23. Theoretical and Experimental Maximum Contact Displacement. .	70
24. Cantilever Beam With an Initial Displacement	80
25. Transverse Impulse to the Free End of a Cantilever Beam. . .	84
26. Transverse Impulse to a Clamped-Clamped Beam at Mid-Span . .	88
27. Initial Velocity Start to a Cantilever Beam.	91
28. Contact Response During Repeated Collisions With a Rigid Body	94

LIST OF SYMBOLS

$y(x,t)$	Displacement
x	Axial beam coordinate
L	Beam length
b	Beam width
h	Beam thickness
d	Separator thickness
$X_j(x)$	Mode (normal) function associated with j th mode
t	Time
E	Modulus of elasticity
I	Moment of inertia
g	Acceleration due to gravity
A	Cross-sectional area of the beam
γ	Weight per unit volume
p_j	Frequency associated with j th mode
y_s	Initial displacement at $x = L$
M	Total mass of beam
ψ	Impulse
m	Specific modal index
n	Number of impact, impact index
e	Coefficient of restitution

\dot{y}

$\partial y / \partial t$

R

Mass ratio

$\delta(t)$

Dirac delta function

δ_{ij}

Kronecker delta

CHAPTER I

INTRODUCTION

Electrical contacts have been the object of the attention of scientists and engineers for many years. However, the advent of the space age and its inherently severe requirements, especially in the area of dynamic environments such as mechanical shock and vibration, has revitalized the study of electrical contacts. Though already at a prodigious level, future environmental requirements will be anything but mitigating. Accompanying the exigency for increased dynamic capability there is an incessant desire for additional miniaturization without a simultaneous degradation in system and component reliability.

Whether the result of a vibration environment or not, unintentional contact transfer has long been one of the undesirable characteristics of switching apparatus employing electrical contact springs. Recent employment of electromechanical switching components in timing and logic circuitry has stimulated interest in another contact nemesis, contact chatter or bounce, the momentary opening of a normally closed circuit. In addition to the inadvertent cessation of circuit continuity, contact chatter can be a primary cause of excessive contact wear and contaminant generation due to arc erosion.

It is paramount that it be kept in mind that loss of continuity and excessive contact wear are only some of the immediate consequences

of contact chatter; the potential ramifications of these phenomena if the contacts are a part of a missile, control system or weapon system, for instance, are overwhelming.

These considerations precipitate a marked need for an understanding of the response of electrical contact springs to various mechanical environments and of the contact chatter phenomenon. This understanding should not be recognized only as a panacea for today's needs and the acquisition of systems capable of surviving and functioning properly but primarily as an incentive for analysis for design and conceptual purposes. Only the delineation, cognizance and understanding of the parameters pertinent to a given device or phenomenon can provide a sound basis for the initiation of design concepts and innovations.

Definition of Problem

The contact spring system shown in Figure 1 is a configuration frequently encountered in components employing electrical contact springs.

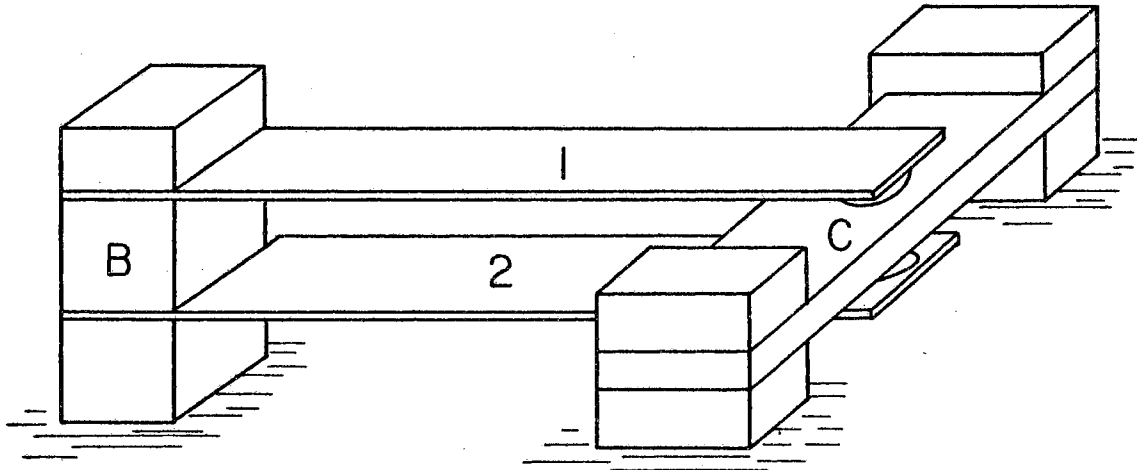


Figure 1. Contact Spring System

The contact system is a redundant one in that circuit continuity from B to C may be provided by contact number 1 or contact number 2. Both B and C are capable of conducting electrical current. Consequently, the simultaneous separation of contact 1 and contact 2, from the contact separator C, is requisite to the occurrence of circuit discontinuity from B to C.

The problem, therefore, is to study the conditions under which the separation of one contact will cause the second contact to leave separator C. The influence of the various system parameters on the occurrence of contact separation may be determined by investigating the conditions under which the release of contact number 1 from some static deflection will cause it to rebound upon collision with C and also induce separation of contact number 2 from C.

The contact springs are assumed to be ideal cantilever springs and separator C to be a clamped-clamped beam. All of the members will be considered to be of homogeneous, isotropic materials and of uniform, prismatic cross sections.

CHAPTER II

PREVIOUS WORK

The primary research effort in the field of electrical contact springs has been conducted from the standpoint of materials, contact resistance, contaminants, electrical arcing and the inherent material transfer [1], [2].

If the electrical contact spring is viewed from the standpoint that it is merely a cantilever beam or a clamped simply supported beam, research in electrical contacts may be interpreted as having commenced with the works of people such as Lord Rayleigh, Euler and Timoshenko. The technical literature abounds with analyses of a multitude of beam configurations and input forcing functions. Unfortunately in all the cases reviewed only the orthodox boundary conditions are considered; that is, a separation or displacement of one of the endpoints of the beam from the foundation is excluded. This latter condition, of course, is intrinsic to contact separation.

In the previous works directly concerned with the dynamic behavior of electrical contact springs most of the early work on contact chatter, which was reviewed, was of a qualitative nature [3], [4], [5], [6], [7], [8], [9]. The case of beam vibration with time dependent boundary conditions has been investigated by Mindlin and Goodman [10]. The time dependent boundary conditions consist of prescribed motions of the beam

supports but separation of the beam from the support is not considered. G. A. Nothmann [11] has analyzed the specific case of the vibration of a cantilever beam with prescribed end motion. The shear forces at the moving end of the beam were investigated but beam separation was precluded. The response to vibration of a propped cantilever beam was analyzed by Peek and Wagar [12], [13] and is described in two sources. Though these works are thorough, separation of the contact from the prop is ignored.

Some investigators have chosen to study the impending separation of two electrical contact springs, that is, to determine the criteria for which separation will occur. These analyses have an obvious advantage in that a lumped system model may be employed. Lowery, Riddle and Stone [14] have studied the separation criteria for a linear set of contacts in a steady-state, sinusoidal vibration environment. Burkhart [15] has made a thorough investigation of the impending separation criteria for the case in which one contact spring has a nonlinear force deflection characteristic and included a qualitative discussion of the effects of damping. An analytical study of the effects of damping for the linear case has been carried out by Baker [16].

Previous works in the specific area of contact chatter have emphasized chatter due to the operation of the device employing the electrical contact springs and have all been done by investigators foreign to the United States, primarily the Japanese.

In France, Pandeile and Tacnet [17] have qualitatively studied the impact and damping problems in a miniature telegraph relay. Also the contact spring configuration studied is of such a specialized nature that it would not be of general interest.

Wikell [18], from Sweden, has treated the response of two electrical contact springs caused by the motion imparted to them as a result of the operation of a relay. The analysis is therefore one of a pair of mating cantilever beams subjected to a prescribed forcing function at their endpoints. The problem is one of finding the solution to a boundary value problem with time-dependent boundary conditions and Wikell's treatment employs the method of Nothmann and that of Mindlin and Goodman, both of which have been previously mentioned. Wikell's analysis results in a delineation of the variation of the contact forces with time thereby permitting the prediction of chatter.

The most extensive and advanced work in contact chatter phenomena has been done by the Japanese. All of their work has been accomplished since about 1955 and is restricted to non-redundant, mating contacts.

Takei [19] has analyzed the displacement due to impact for a single degree of freedom system using Jacobsen's phase-plane techniques. This analysis has limited application due to the restriction to a single degree of freedom, and electrical contact springs are almost without exception distributed, infinite degree of freedom, elastic systems.

A statistical approach, based on the factorial design of experiments, has been employed by Shinohara, Ohki and Takashi [20] to study the transverse vibration of two cantilevers. This analysis is strongly oriented towards the analysis of switches of the sealed, dry reed variety. The relations governing the interdependence of the various contact spring parameters are not the result of a theoretical derivation but are the consequence of an empirical examination of the chatter phenomenon for the case of two cantilever beams. As a result the relations are of a

qualitative nature and the problem parameters are given a statistical level of significance resulting from the factorial design analysis.

In an effort to extend the analysis of Takei [19], mentioned earlier, Takei and Takashi [21] have applied the graphical phase-plane technique to the contact chatter resulting from the interaction of two cantilever beams, taking the higher modes of the cantilever beams into account. The use of the graphical phase-plane technique is most advantageous for nonlinear and single degree of freedom problems; it becomes quite cumbersome when applied to the situation at hand. Though the principle of superposition may be applied to the manipulation of the vibrational modes, for the linear case, it is not practical to construct the trajectories for various modes independently when the possibility of impact exists. It may be possible to apply the digital computer method for the phase-plane technique developed by Simpson [22] to make this approach more expeditious.

The most notable and extensive work reviewed was that of Takamura, Shimizu and Otuka [23]. It is actually the first paper dealing with the repeated collisions between two bodies as is the case in the chatter of electrical contacts. A general discussion of the theory of the vibrations caused by the collision between two elastic bodies is presented and the response of a single degree of freedom or an elastic body colliding with a rigid body is investigated. Takamura, et al. employed an analog computer for this analysis.

Previous investigations in the area of impact and stress wave propagation appear to have been motivated primarily by a desire to study either the mechanism of wave propagation itself or the properties of

materials. For this reason, naturally only the optimum models and test specimen configurations have been used. Analyses are usually done on rods or prismatical bars with the loading forces distributed across the entire cross-sectional face of the bar or rod.

Prior to mentioning any specific technical papers three basic works in this area should be mentioned, namely those of Hertz [24], Goldsmith [25] and Kolsky [26]. Early authorities on the theory of impact, such as Love and Timoshenko [27], [28] and their respective treatises on the theory of elasticity should also be noted.

Ripperger [29], Davidson and Meier [30], and Donnell [31] have prepared comprehensive works on the various aspects of the longitudinal impact of bars and the attendant wave phenomena. Cunningham and Goldsmith [32] have documented an experimental investigation of the impulses resulting from the longitudinal impact of a steel ball on narrow rectangular bars.

If a departure from the realm of convenient specimen geometries and loadings is made and the literature pertaining to concentrated impulsive loadings on geometries such as plates is sought, one is brought to the startling conclusion that very little analysis has been done. The investigations reviewed which were close to this problem both treated a concentrated impulsive load applied to a semi-infinite medium. Morse [33] treats the problem of compressional waves in a member of rectangular cross section; however, no mention is made that loadings and restrictions are placed on the cross-sectional dimensions so as to place it in the class of a rod.

The most notable work is that of Broberg [34] in which he develops a theory, using the Hertz law of contact, suitable for solving for the

displacement, along the axis of symmetry, of a semi-infinite elastic solid and the line of an applied impulsive force directed normal to the half-space at the free surface.

In Broberg's thesis, which contains extensive experimental work as well as some elaborate mathematical analysis, the impulsive force is the result of either a detonated explosive charge in contact with the free surface or the shooting of a projectile (sphere) against the free surface of the half-space.

The subject of the impact of a mass on a beam has been investigated with renewed interest in recent years; however, almost all the works reviewed had two convenient constraints applied, specifically:

1. Only simply-supported beams were analyzed.
2. Impact considered was always between a solid mass and an elastic beam rather than an impact between members which have distributed elasticity.

The early treatises on the impact of a mass on an elastic beam were the result of the efforts of the well-known researchers, Saint Venant [38], Timoshenko [39], and Rayleigh [40]. All of these works applied energy methods to the problem and also made the assumption that the striking mass becomes an integral part of the beam subsequent to collision. These analyses, as well as all those to be described, assume the contact force theories developed by Hertz [24], [41] to be applicable.

Lee [42] has considered the impact of a mass striking a beam with the added complexity of rebound of the impacting mass following the collision. Subject to the assumption of a linear velocity for the mass and that the resulting vibrations of the beam are confined to the first

normal mode of the beam, the relations necessary to predict the deflection of the beam are derived for central impact on a uniform simply-supported beam.

The analysis of the central impact of a mass on a simply-supported beam including the consideration of internal and external damping has been carried out by Hoppmann [43]. The contact force is considered as a function of time and the effect of the beam resting on an elastic foundation is discussed.

Dengler and Goland [44] have approached the transverse impact problem from more of an elasticity approach and arrived at a closed solution for the stresses induced in a uniform beam due to the application of a concentrated, impulsive transverse load. By using the Laplace transformation techniques and basing the solution on the Timoshenko beam equation rather than the Euler beam equation, they have included the effects of rotatory inertia and shear. The beam is taken to be of infinite length and the closed solution is valid only when the beam's elastic properties are such that the transverse shear modulus and the Young's modulus are equal.

The analysis of the flexural displacements of a beam and plate due to a transverse, concentrated, time-dependent force, is presented in a paper by Eringen [45]. The force again is that due to the impact of a mass on a beam and Hertz's law of impact is applied. Eringen, however, delves into the problem of the shape of the force versus time curve in greater detail than previous authors. The force is normally assumed to have a sinusoidal variation with time or to obey an equation comprised of a polynomial of sine terms. Eringen indicates that the

deflection is practically independent of the shape of the contact force function. He found the deflections obtained using a Dirac δ -function to be in good agreement, providing the impulse delivered to the beam is consistent for the Dirac and time-dependent forces. This presents a major simplification in the complexity of the analysis especially when Laplace transform techniques are applied.

Boley has been a major contributor to the literature on the problem of the impacting of a mass on a beam having contributed three recent papers in this area. The initial work was an independent effort by Boley while the latest two papers were co-authored with C. C. Chao.

In Boley's paper [46] an approximate theory is developed for the analysis of the behavior of a Timoshenko beam subjected to a transverse impact. Boley also attacked the problem from an elastician's standpoint and used a "travelling-wave" approach to analyze a section of the beam which undergoes a sudden change in shear force. Though not explicitly stated, the beam is assumed to be semi-infinite in length.

The first work presented by Boley and Chao [47] applied the method of Laplace transforms to a beam obeying the Timoshenko model and subjected to four types of dynamic loadings. All the loadings have a single characteristic in common; namely, they are concentrated at a single longitudinal location on the beam. Once more the analysis is based on a semi-infinite beam. Solutions are presented in terms of definite integrals which must be evaluated numerically.

The second work co-authored by Boley and Chao [49] is based, for all practical purposes, on the original work by Boley. This paper proposes a method of analyzing a beam of finite length, a simply-supported

beam, by applying the technique of superposition to the previous semi-infinite results.

Goldsmith and Cunningham [49] have reported some interesting experimental effort on the kinetics of oblique impact on beams. The impact of a 1/2-inch diameter steel ball on steel beams was investigated by means of a Fastex camera. The beams were of 22 and 30 inch spans, clamped, and simply-supported respectively. Beam deflection as well as crater topography were studied. This paper, though terse in its presentation, was found to be very detailed, unambiguous and extremely informative.

CHAPTER III

MATHEMATICAL MODEL

The analysis of the contact separation phenomenon in the redundant contact system, depicted in Figure 2, may be divided into the following four subproblems:

- A. The transverse vibrational response of the upper contact spring after release from the initial static deflection y_s and the subsequent collision with the separator.
- B. Transmission of the impulse due to the impact of the upper contact with the contact separator to the lower contact spring.
- C. Transverse vibrational response of the lower contact spring to an initial velocity from the contact separator.
- D. Analysis for determination of the impulse resulting from the collision of the upper contact with the separator.

The governing relation for the maximum displacement of the lower contact will then provide a basis for determining the system parameters which influence the magnitude of the contact separation as well as their interdependence. In addition, it should furnish a basis for selecting the preload for the lower contact.

Transverse Vibrational Response of Upper Contact Spring

The upper contact spring is assumed to be a linear, undamped, elastic cantilever beam whose behavior is governed by the Bernoulli-Euler beam

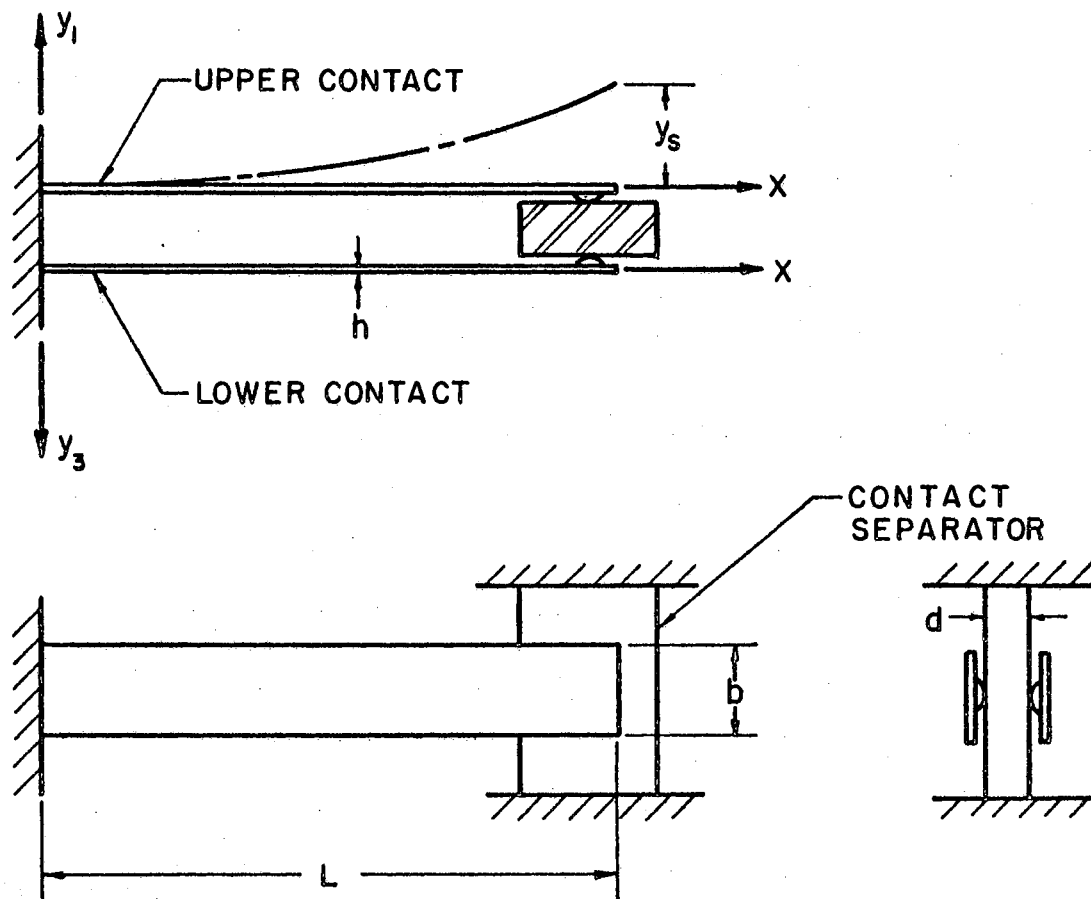


Figure 2. Theoretical Model

equation. This implies the existence of perfect clamped boundary conditions at $x = 0$, as well as insignificant shear and rotatory inertia effects during transverse flexure of the beam.

The Bernoulli-Euler beam equation for the displacement, $y(x,t)$, of a beam during transverse, flexural vibrations is

$$a^2 \frac{\partial^4 y(x,t)}{\partial x^4} + \frac{\partial^2 y(x,t)}{\partial t^2} = 0. \quad (1)$$

The solution of equation (1) is well known [35], [36] and represents the free vibrations of the beam, restricted to the x-y plane; namely,

$$y(x,t) = \sum_{j=1}^{\infty} X_j(x) \cdot \varphi_j(t),$$

or,

$$y(x,t) = \sum_{j=1}^{\infty} X_j(x) (A_j \cos p_j t + B_j \sin p_j t) \quad (2)$$

where $X_j(x)$ = normal mode function, and

$$a^2 = EI_g/A\gamma.$$

Substitution into the boundary conditions,

$$X(0) = 0$$

$$X'(0) = 0$$

$$X''(L) = 0$$

$$X'''(L) = 0$$

yields values for the constant coefficients in the mode function as well as the frequency equation

$$\cos kL \cosh kL = -1$$

where $k = \sqrt{p/a}$. The coefficients A_j and B_j are determined by the initial conditions on the cantilever beam.

For the present analysis the initial conditions are as follows

$$y(x,0) = f(x)$$

$$y(L,0) = y_s$$

$$\dot{y}(x,0) = 0.$$

The selection of the function, $f(x)$, which describes the shape or curvature of the cantilever beam prior to its release, is very significant. Since the initial velocity is zero the coefficients, B_j in equation (2), will be zero. The remaining coefficients, A_j , will therefore be determined solely by the choice of $f(x)$.

Thus far, the only constraint which has been placed on the initial beam configuration is that $y(L,0) = y_s$. In this analysis the initial curvature will be assumed to be the consequence of a force at $x = L$ of sufficient magnitude to satisfy the constraint $y(L,0) = y_s$. The function $f(x)$ will then be the static deflection curve for a cantilever beam subjected to a static force at its free end, which from strength of materials theory is

$$f(x) = \frac{3y_s}{L^3} \left[\frac{Lx^2}{2} - \frac{x^3}{6} \right].$$

The displacement response of the cantilever beam subsequent to release from the initially deflected position may be shown to be (see Appendix A),

$$y(x,t) = \sum_{j=1}^{\infty} A_j X_j(x) \cos p_j t. \quad (3)$$

The velocity is then given by

$$\dot{y}(x,t) = \sum_{j=1}^{\infty} -p_j A_j X_j(x) \sin p_j t \quad (4)$$

where the coefficients A_j are given by

$$A_j = \frac{3y_s}{L^2} \int_0^L \left(\frac{Lx^2}{2} - \frac{x^3}{6} \right) X_j(x) dx. \quad (5)$$

The equations (3) through (5) delineate the beam behavior until the moment the free end of the beam impacts with the separator; that is, when $y(L,t) = 0$. At this instant both the contact separator and the free end of the beam will experience an impulse ψ due to the impact. The response of a cantilever beam subjected to an impulse at its free end is (see Appendix B)

$$y(x,t) = \frac{\psi}{M} \sum_{j=1}^{\infty} \frac{X_j(x) X_j(L)}{p_j} \sin p_j t \quad (6)$$

and differentiation of (6) yields the beam velocity response, namely

$$\dot{y}(x,t) = \frac{\psi}{M} \sum_{j=1}^{\infty} X_j(x) X_j(L) \cos p_j t. \quad (7)$$

Therefore the total displacement response of the beam subsequent to impact is,

$$y(x,t) = \sum_{j=1}^{\infty} \left\{ A_j \cos p_j t + \left[B_j - \frac{\psi}{M} \frac{X_j(L)}{p_j} \right] \sin p_j t \right\} X_j(x) \quad (8)$$

and the total velocity expression after impact is,

$$\dot{y}(x,t) = \sum_{j=1}^{\infty} \left\{ -A_j \sin p_j t + \left[B_j - \frac{\psi}{M} \frac{X_j(L)}{p_j} \right] \cos p_j t \right\} \cdot p_j X_j(x). \quad (9)$$

In addition to the unknown coefficients A_j and B_j , which now depend on the initial conditions immediately before impact, the impulse is also to be determined. The derivation of an expression for ψ is deferred until Section D when the necessary response equations are available.

The analysis of the displacement response of the top contact, subject to an assumed collision between the top contact and a flexurally rigid separator, is presented in Appendix E. This analysis will predict the displacement versus time history of the contact including the first and subsequent collisions. A general recursion relation is derived to relate the coefficients A_{jn} and B_{jn} , for the n th impact, in terms of $A_{j(n-1)}$ and $B_{j(n-1)}$.

Transmission of the Impulse by the Contact Separator

The analysis of the transmission of the impulse delivered to the contact separator by the upper contact spring presents a particular problem.

Two phenomena may be present as a result of the incident impulse, namely the transmission of a stress wave through the separator from the point of application of the impulse and the flexural response of the separator as a clamped-clamped beam. If the separator is assumed to be flexurally rigid, the stress wave mechanism will predominate and this analysis will be treated next.

As was mentioned previously the major difficulty arises from the geometry of the separator. The configuration is as shown in Figure 3a.

The actual system, shown in Figure 3a, has a concentrated impulse delivered to the center of a plate of finite thickness. The impulse will initiate a stress wave in the separator plate which will propagate from $(x,y,z) = (0,0,0)$ in the positive z direction. As the dilatational wave passes through the separator the medium will experience a particle motion and hence a velocity in the direction of wave propagation. The

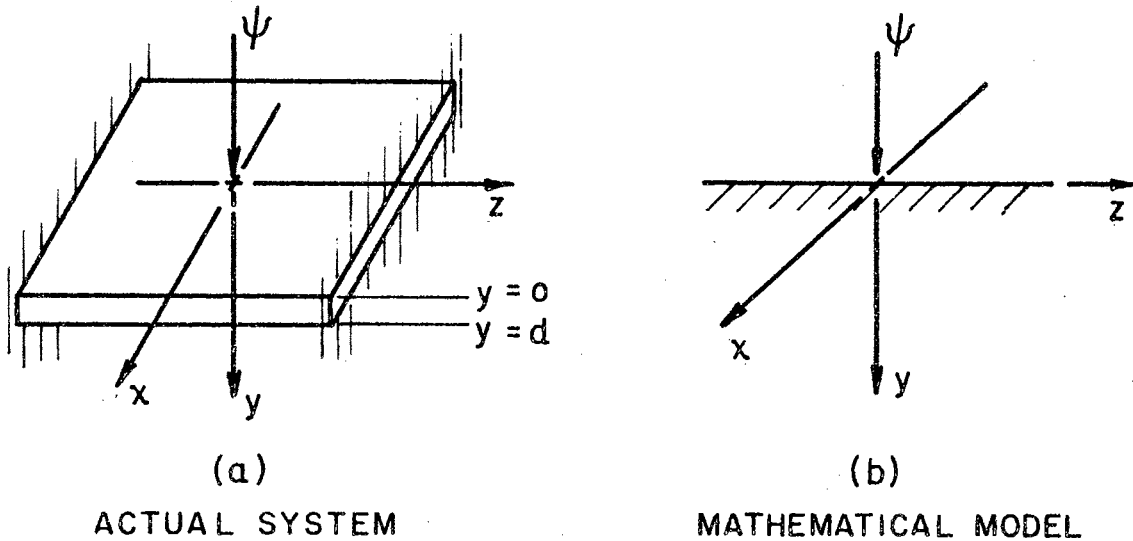


Figure 3. Impulse to the Contact Separator

dilatational wave will traverse the separator with dilatational wave velocity, c_d , and upon impinging the surface $y = d$ will cause a displacement of the surface particles and therefore the bottom contact which is contiguous with the separator at $(x,y,z) = (0,d,0)$.

The analysis of the transmission of the wave through the contact separator may be simplified significantly by considering the mathematical model shown in Figure 3b. The separator, of finite thickness d , has been replaced by a semi-infinite medium. The impulse ψ is delivered at coordinates $(0,0)$ of the x - z plane which is the free surface of the half-space.

It is possible to apply this simplified mathematical model to approximate the actual configuration by evaluating the particle displacement at a specific y coordinate, namely that corresponding to the separator thickness or $y = d$. However, at $y = d$ the wave encounters the boundary of the contact separator, a free surface, and is reflected

which results in the particle displacements and hence the particle velocities being twice the corresponding values in the semi-infinite body. This particle velocity then becomes the initial velocity start imparted to the bottom contact spring at its free end.

The equation for the particle displacement u_d at a particular coordinate $(0,d,0)$ of a homogeneous, elastic half-space is [34],

$$u_d = \frac{\psi}{2\pi\delta^c d^2} \delta\left(\frac{c_d t - 1}{d}\right) . \quad (10)$$

For a free boundary at $y = d$, u_d would be doubled and the particle velocity obtained by taking the time derivative.

The magnitude of this velocity, which would be imparted to the bottom contact, is exceedingly small and is insufficient to cause the responses of the lower contact noted in experiments. There is also definite indication of significant flexural response of the separator and it will be assumed that this is the transfer mechanism.

The displacement response of the contact separator as a clamped-clamped beam subjected to an impulse at mid-span is given by (see Appendix C),

$$y(x,t) = \frac{\psi g}{\gamma AL} \sum_{j=1}^{\infty} X_j(L/2) \frac{X_j(x)}{p_j} \text{Sin } p_j t . \quad (11)$$

The velocity response is derived by differentiating equation (11) with respect to time t and is,

$$\dot{y}(x,t) = \frac{\psi g}{\gamma AL} \sum_{j=1}^{\infty} X_j(L/2) X_j(x) \text{Cos } p_j t . \quad (12)$$

Evaluation of equation (12) at the midpoint, $x = L/2$ of the separator will then yield the initial velocity for the lower contact.

Transverse Vibrational Response of Lower Contact

The response of the lower contact spring can be developed in much the same manner as the upper contact except for its initial conditions. From the previous section it is seen that the free end will experience an initial velocity due to the flexural velocity attained by the separator at $x = L/2$. Consider the system shown in Figure 4.

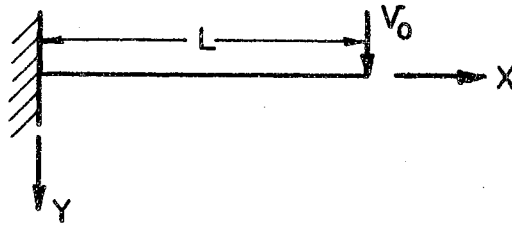


Figure 4. Initial Velocity Start to A Cantilever Beam

The initial conditions are,

$$y(x,0) = 0; \dot{y}(x,0) = \begin{cases} 0, & \forall x \neq L \\ v_0, & \forall x = L \end{cases} .$$

The initial conditions on velocity may be expressed conveniently, using the Dirac Delta function, as $\dot{y}(x,0) = v_0 \delta(x-L)$.

The displacement response of a linear, elastic cantilever beam to an initial velocity at its free end is (see Appendix D),

$$y(x,t) = \sum_{j=1}^{\infty} \frac{v_0}{L} \frac{X_j(L)}{p_j} X_j(x) \text{Sin } p_j t . \quad (13)$$

The corresponding velocity expression is therefore,

$$\dot{y}(x,t) = \sum_{j=1}^{\infty} \frac{v_0}{L} X_j(L) X_j(x) \text{Cos } p_j t . \quad (14)$$

Subject to the notation presented in Appendix E, equations (13) and (14) are valid in the time interval $0 \leq t \leq t_1$. At $t = t_1$ the first impact occurs and the boundary conditions must again be imposed. For displacement,

$$y_0(x, t_1^-) = y_1(x, t_1^+) = y_1(x, 0),$$

which yields

$$\begin{aligned} & \sum_{j=1}^{\infty} \frac{v_0}{L} \frac{X_j(L) X_j(x)}{p_j} \sin p_j t_1 \\ &= \sum_{j=1}^{\infty} \left\{ A_{j_1} \cos p_j t_1^+ + \left[B_{j_1} - \frac{\psi_1}{M} \frac{X_j(L)}{p_j} \right] \sin p_j t_1^+ \right\} X_j(x) \\ &= \sum_{j=1}^{\infty} A_{j_1} X_j(x). \end{aligned}$$

Thus the relation for the coefficient A_{j_1} is,

$$A_{j_1} = \frac{v_0}{L} \frac{X_j(L)}{p_j} \sin p_j t_1. \quad (15)$$

The velocities before and after impact are related as,

$$\dot{y}_1(L, t_1^+) = \dot{y}_0(L, t_1^-) - \frac{\psi_1}{M} \sum_{j=1}^{\infty} X_j^2(L)$$

which, upon substitution for the velocities becomes,

$$\begin{aligned} & \sum_{j=1}^{\infty} p_j X_j(L) \left[B_{j_1} - \frac{\psi_1}{M} \frac{X_j(L)}{p_j} \right] \\ &= \sum_{j=1}^{\infty} \frac{v_0}{L} X_j(L) X_j(L) \cos p_j t_1 - \frac{\psi_1}{M} \sum_{j=1}^{\infty} X_j^2(L). \end{aligned}$$

The coefficients, B_{j_1} , may therefore be calculated from the following expression,

$$B_{j_1} = \frac{v_0}{L} \frac{X_j(L)}{p_j} \cos p_j t_1. \quad (16)$$

The response of the beam for $t_1 \leq t \leq t_2$ is therefore,

$$y(x,t) = \sum_{j=1}^{\infty} \left\{ A_{j_1} \cos p_j t + \left(B_{j_1} - \frac{\psi_1}{M} \frac{X_j(L)}{p_j} \right) \sin p_j t \right\} X_j(x) \quad (17)$$

where the coefficients A_{j_1} and B_{j_1} are given by equations (15) and (16), respectively.

For $t \geq t_2$, the vibrational response of the lower contact may be analyzed just as the top spring in part A; that is, equations (7), (8), and (9) of Appendix E are valid expressions for the beam displacement.

Derivation of the Impulse Expression

The analysis will assume that the collision is between two elastic bodies one of which is the top contact and the second is the contact separator and the lower contact. The entire phenomenon can be described by the three conservation relationships:

- (1) Conservation of Mass
- (2) Conservation of Momentum
- (3) Conservation of Energy.

The conservation of mass is obviously satisfied. If the conservation of momentum and energy are applied to the collision of two elastic bodies of mass, M_1 and M_2 , traveling with velocities v_1 and v_2 respectively, prior to collision, the expression for the impulse is given by

$$\psi = (1 + e) \frac{(v_{1-} - v_{2-})}{\frac{1}{M_1} + \frac{1}{M_2}} \quad (18)$$

The symbol e is the coefficient of restitution defined by

$$e = \frac{v_{2+} - v_{1+}}{v_{1-} - v_{2-}} ; 0 < e < 1,$$

and is a measure of the "elasticity" of the impact.

For the case of the impact of the distributed members involved in this analysis, an impulse expression may be derived from the conservation of energy relationship. This approach will inherently assume that,

1. Collision is perfectly elastic or the energy of plastic deformation is negligible.
2. At the instant of impact the significant form of energy is kinetic energy.

The kinetic energy will be given by $\frac{M_i \dot{y}_i^2}{2}$, $i = 1, 2, 3$, where the subscripts will refer to the upper contact, separator and lower contact, respectively. The superscripts plus (+) and minus (-) refer to the time immediately after and before collision. The respective kinetic energies may then be given by the following expressions:

$$\frac{M_1 (\dot{y}_1^-)^2}{2} = \frac{M_1}{2} \int_0^L \left[\sum_{j=1}^{\infty} p_j A_j X_j(x) \sin p_j t^- \right]^2 dx,$$

$$\begin{aligned} \frac{M_1 (\dot{y}_1^+)^2}{2} &= \frac{M_1}{2} \int_0^L \left\{ \sum_{j=1}^{\infty} [-A_j \sin p_j t^+ \right. \\ &+ (B_j - \frac{\psi}{M_1} \frac{X_j(L_1)}{p_j}) \cos p_j t^+ \left. \right] X_j(x) p_j \left. \right\}^2 dx, \end{aligned}$$

$$\frac{M_2(\dot{y}_2^-)^2}{2} = 0; \quad \frac{M_3(\dot{y}_3^-)^2}{2} = 0,$$

$$\frac{M_2(\dot{y}_2^+)^2}{2} = \frac{M_2}{2} \int_0^L \left[\frac{\psi}{M_2} \sum_{j=1}^{\infty} X_j(L_2/2) X_j(x) \cos p_j t^+ \right]^2 dx,$$

$$\frac{M_3(\dot{y}_3^+)^2}{2} = \frac{M_3}{2} \int_0^L \left[\frac{\psi}{M_3} \sum_{j=1}^{\infty} X_j(L_3) X_j(x) \cos p_j t^+ \right]^2 dx.$$

If the total kinetic energies immediately before and after impact are equated and the substitution, $t^+ = 0$, is made, the resulting equation is,

$$\begin{aligned} & \frac{M_1}{2} \int_0^L \left[\sum_{j=1}^{\infty} -p_j A_j X_j(x) \sin p_j t^- \right]^2 dx \\ &= \frac{M_1}{2} \int_0^L \left[\sum_{j=1}^{\infty} \left(B_j - \frac{\psi}{M_1} \frac{X_j(L_1)}{p_j} \right) p_j X_j(x) \right]^2 dx \\ &+ \frac{M_2}{2} \int_0^L \left[\sum_{j=1}^{\infty} \frac{\psi}{M_2} X_j(L_2/2) X_j(x) \right]^2 dx \\ &+ \frac{M_3}{2} \int_0^L \left[\sum_{j=1}^{\infty} \frac{\psi}{M_3} X_j(L_3) X_j(x) \right]^2 dx \end{aligned}$$

If, in the preceding equation, the quantities to be squared are expanded, the integration and summations are inverted and the orthogonality condition applied; the expression for the impulse is found to be,

$$\psi = 2 \frac{\sum_{j=1}^{\infty} p_j B_j X_j(L)}{\sum_{j=1}^{\infty} \frac{X_j^2(L_1)}{M_1} + \frac{X_j^2(L/2)}{M_2} + \frac{X_j^2(L)}{M_3}} \quad (19)$$

Since the quantity $\sum_{j=1}^{\infty} p_j B_j X_j(L)$ is actually the impact velocity of the top contact and the coefficient of restitution by definition is such that $0 \leq e \leq 1$, it is noted that equation (19) is analogous to equation (18). It will be assumed that the restriction on the magnitude of e also applies for a collision of elastic bodies in which the vibration of the colliding bodies is not negligible. Hence, the general expression for the impulse is given by,

$$\psi = \frac{(1 + e) \sum_{j=1}^{\infty} p_j B_j X_j(L)}{\sum_{j=1}^{\infty} \frac{X_j^2(L)}{M_1} + \frac{X_j^2(L/2)}{M_2} + \frac{X_j^2(L)}{M_3}} \quad (20)$$

where the applicable mode function must be chosen for the respective beams and also be evaluated at the appropriate length L .

CHAPTER IV

ANALYSIS AND DISCUSSION OF THE EQUATIONS

CONSTITUTING THE MATHEMATICAL MODEL

As stated in the Introduction, it is only the delineation, cognizance and understanding of the pertinent parameters of a system which will yield valid, fruitful modifications and innovations to a system design. It is the intention of this thesis to provide the aforementioned information with regard to the redundant contact system and the phenomenon of contact separation in that system.

In this chapter a discussion of the equations derived in the previous chapter will be presented. The interrelation of the system parameters, as far as the displacement response of the lower contact is concerned, will be scrutinized to indicate the system parameters which are available to the designer in his quest to eliminate circuit discontinuity or simultaneous separation of the upper and lower contacts from the contact separator.

In an actual contact design or a revision to a design it is essential that the effect of the various system parameters on the magnitude of the contact displacement be known. This information is equally vital in determining meaningful manufacturing tolerances for the contact system. Thus, the following discussion should perhaps be motivated by the question, "What modifications to the system may be adopted to minimize the displacement of the lower contact?".

The system parameters are subscripted 1, 2, and 3 to indicate the upper contact, contact separator and the lower contact, respectively.

Governing Equation

The governing equation for the displacement of the lower contact at its free end,

$$y_3(L_3, t) = \sum_{j=1}^{\infty} \frac{v_0 X_{j_3}^2(L_3)}{L_3 p_{j_3}} \sin p_{j_3} t$$

may be rewritten by substituting for the velocity v_0 with,

$$v_0 = \frac{\psi g}{\gamma_2 A_2 L_2} \sum_{j=1}^{\infty} X_{j_2}^2(L_2/2) = \frac{\psi}{M_2} \sum_{j=1}^{\infty} X_{j_2}^2(L_2/2)$$

where

$$\psi = \frac{(1+e) \sum_{j=1}^{\infty} p_{j_1} B_{j_1} X_{j_1}}{\sum_{j=1}^{\infty} \frac{X_{j_1}^2(L_1)}{M_1} + \frac{X_{j_2}^2(L_2/2)}{M_2} + \frac{X_{j_3}^2(L_3)}{M_3}}$$

The resulting equation is

$$y_3 = \frac{(1+e)}{L_3 M_2} \cdot \frac{\left[\sum_{j=1}^{\infty} X_{j_2}^2(L_2/2) \right] \left[\sum_{j=1}^{\infty} p_{j_1} B_{j_1} X_{j_1} \right]}{\sum_{j=1}^{\infty} \frac{X_{j_1}^2(L_1)}{M_1} + \frac{X_{j_2}^2(L_2/2)}{M_2} + \frac{X_{j_3}^2(L_3)}{M_3}} \quad (21)$$

$$\sum_{j=1}^{\infty} \frac{X_{j_3}^2(L_3)}{p_{j_3}} \sin p_{j_3} t$$

It would at first appear that this expression is independent of the initial displacement; however, it should be recalled that B_{j_1} is determined by the initial displacement of the upper contact as outlined in Part A of Chapter III. For convenience and to preclude the omission of the initial displacement of the upper contact in the discussion, the definition

$$B_{j_1} = \frac{y_s}{L_1} C_{j_1}$$

is introduced, where y_s is the static, initial displacement of the free end of the upper contact. With the above substitution equation (21) may be written as

$$y_3 = \frac{(1+e)y_s}{L_3 L_1 M_2} \cdot \frac{\left[\sum_{j=1}^{\infty} X_{j_2}^2(L_2/2) \right] \left[\sum_{j=1}^{\infty} p_{j_1} C_{j_1} X_{j_1}(L_1) \right]}{\sum_{j=1}^{\infty} \frac{X_{j_1}^2(L_1)}{M_1} + \frac{X_{j_2}^2(L_2/2)}{M_2} + \frac{X_{j_3}^2(L_3)}{M_3}} \quad (22)$$

$$\sum_{j=1}^{\infty} \frac{X_{j_3}^2(L_3)}{p_{j_3}} \sin p_{j_3} t .$$

This equation yields the specific solution for the displacement versus time of the free end of the lower contact, that is, $y_3(L_3, t)$.

It should be noted that equation (22) has been particularized for the contact configuration to be studied in this thesis. The solution is not general in that the normal mode functions are dictated by the specific types of distributed members which comprise the specific system under analysis. In addition, the normal mode functions, $X_{j_i}(x_i)$, are evaluated at the beam coordinates, x_i , at which the impact

occurs in this particular configuration. However, the basic analysis is completely general since there are no constraints applied to the normal mode functions or the location at which the mode function is evaluated. Thus the basic analysis is completely general as far as configuration is concerned and may be applied to any system comprised of three uniform prismatic members, with distributed elasticity, which obey the Bernoulli-Euler beam equation.

Equation (22) may be written as follows

$$y_3(x_3, t) = \frac{(1 + e)y_s}{L_1 L_3 M_2} \cdot \frac{\left[\sum_{j=1}^{\infty} X_{j_2}^2(x_2) \right] \left[\sum_{j=1}^{\infty} p_{j_1} C_{j_1} X_{j_1}(x_1) \right]}{\sum_{j=1}^{\infty} \frac{X_{j_1}^2(x_1)}{M_1} + \frac{X_{j_2}^2(x_2)}{M_2} + \frac{X_{j_3}^2(x_3)}{M_3}} \cdot \sum_{j=1}^{\infty} \frac{X_{j_3}^2(x_3)}{p_{j_3}} \sin p_{j_3} t . \quad (23)$$

This equation is completely general and each of the three distributed members can be any of the orthodox beam configurations as long as the respective mode functions, $X_{j_i}(x_i)$, are chosen correctly. In addition the point of contact of the three members is completely variable, that is, the mode function X_{j_i} of the i th body may be evaluated at the general axial coordinate x_i corresponding to the points at which the members are contiguous. The possibility of such a generalization should present a strong motivation for analyzing such configurations as the distributed systems they in actuality are.

In several of the works reviewed which deal with contacts, especially those which hypothesize a lumped-parameter, single degree of freedom contact model, the model is usually studied by varying the spring constants, masses and their ratios. These studies allow the magnitude of the contact mass and spring stiffness to vary independently. Though this condition provides the analyst with a mechanism with which to study the contact system it is an opportunity rarely afforded the designer when choosing a contact configuration. It is true that a contact system may respond predominantly in a single mode, given the proper excitation, but it is also true that most contacts are not single degree of freedom systems. This is not to say that it is impossible to vary the contact spring constant and simultaneously maintain an invariant contact mass, but rather that it would be an infrequent luxury.

The use of a distributed parameter model, necessary in this analysis due to the impact, provides an improved insight into contact response but unfortunately produces a relation of the complexity of equation (22). The governing equation, with its inherent algebraic series, does not lend itself to immediate conclusions as to the interactions of the various system parameters.

Coefficient of Restitution and Initial Deflection

To return to the specific system at hand, equation (22) delineates the relationship of the various system parameters and will afford the designer the opportunity to study effects of varying these parameters on the magnitude of the displacement of the lower contact. As it is

desirable to minimize this displacement, it can be seen that both the initial static deflection, y_s , and the coefficient of restitution, e , should be minimized. The coefficient of restitution, though definitely a design variable, is an elusive one in that the factors which determine its magnitude are not clearly definable and can only be discussed qualitatively. This parameter will be discussed further in Chapter VI. For the present discussion, the coefficient of restitution might best be described as a measure of the efficiency of the impact which occurs in the system. Thus, the requirement that the coefficient of restitution be minimized is equivalent to desiring as inefficient an impact as possible within the remaining design constraints.

A graph depicting the maximum displacement of the lower contact, y_3 as a function of the contact separator thickness, h , is shown in Figure 5. Three curves for three different values of the initial static displacement, y_s , of the upper contact have been shown. This plot indicates, as does the mathematical model, that the magnitude of the lower contact response decreases with decreasing initial displacement. The plot also indicates that the lower contact response approaches the ordinate, $y_3 = 0$, as the contact separator thickness increases. Thus the magnitude of the separation of the lower contact may be reduced by reducing the initial static displacement and by increasing the thickness of the contact separator.

Normal Mode Function

The normal mode function presents a design parameter which is frequently overlooked. The shape of the normal modes is determined

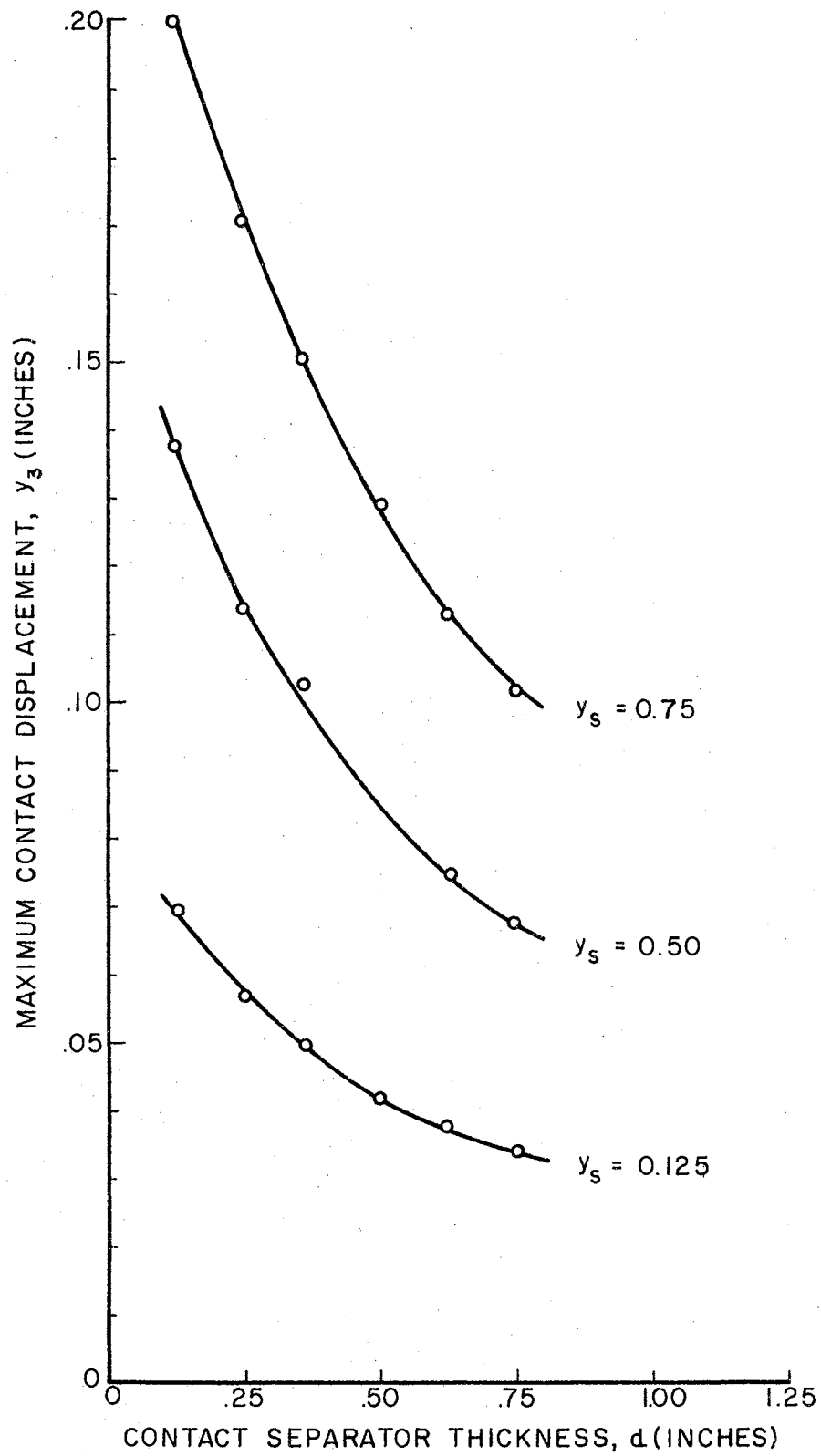


Figure 5. Theoretical Values of the Maximum Contact Displacement Versus Contact Separator Thickness

solely by the boundary conditions on the beam and for this reason once the beam has been classified the normal modes are usually assumed to be of no design value. It is true that the modes are fixed at this time; however, the modes are also a function of x , the axial coordinate of the beam. Thus, since the mode functions are periodic functions there exists the possibility that the summation of the mode functions will have finite maxima, minima, and nodes when evaluated with the axial beam coordinate as the independent variable.

However, the dependence of the displacement of the lower contact on the magnitude of the mode functions is not obvious from equation (22). Figure 6 shows a plot of the lower contact displacement versus the ratio of x_3/L_3 with $x_2/L_2 = 0.5$. An additional restriction placed on the ratio of x_3/L_3 was that it lie in the range $0.7 \leq x_3/L_3 \leq 1.0$. This constraint was applied since in an actual application an electrical contact is made at a point where the contact has minimum stiffness. For a cantilever contact this implies that it be as close to the free end as is practical. The minimum value in the range of x_3/L_3 was chosen to include the first nodal point of the contact's second mode and consequently the first nodal point of all the other modes.

Curve I indicates the variation in the contact displacement, y_3 , as a function of x_3/L_3 with the total contact length, L_3 , remaining invariant. In curve II the length of the contact was increased by an amount equal to $(1-x_3/L_3)L_3$ at each x_3/L_3 . This is equivalent to allowing x_3/L_3 to vary while maintaining a constant axial location of the point of abutment from the contact support. It was hoped that this would maintain a constant contact stiffness. However, the stiffness was

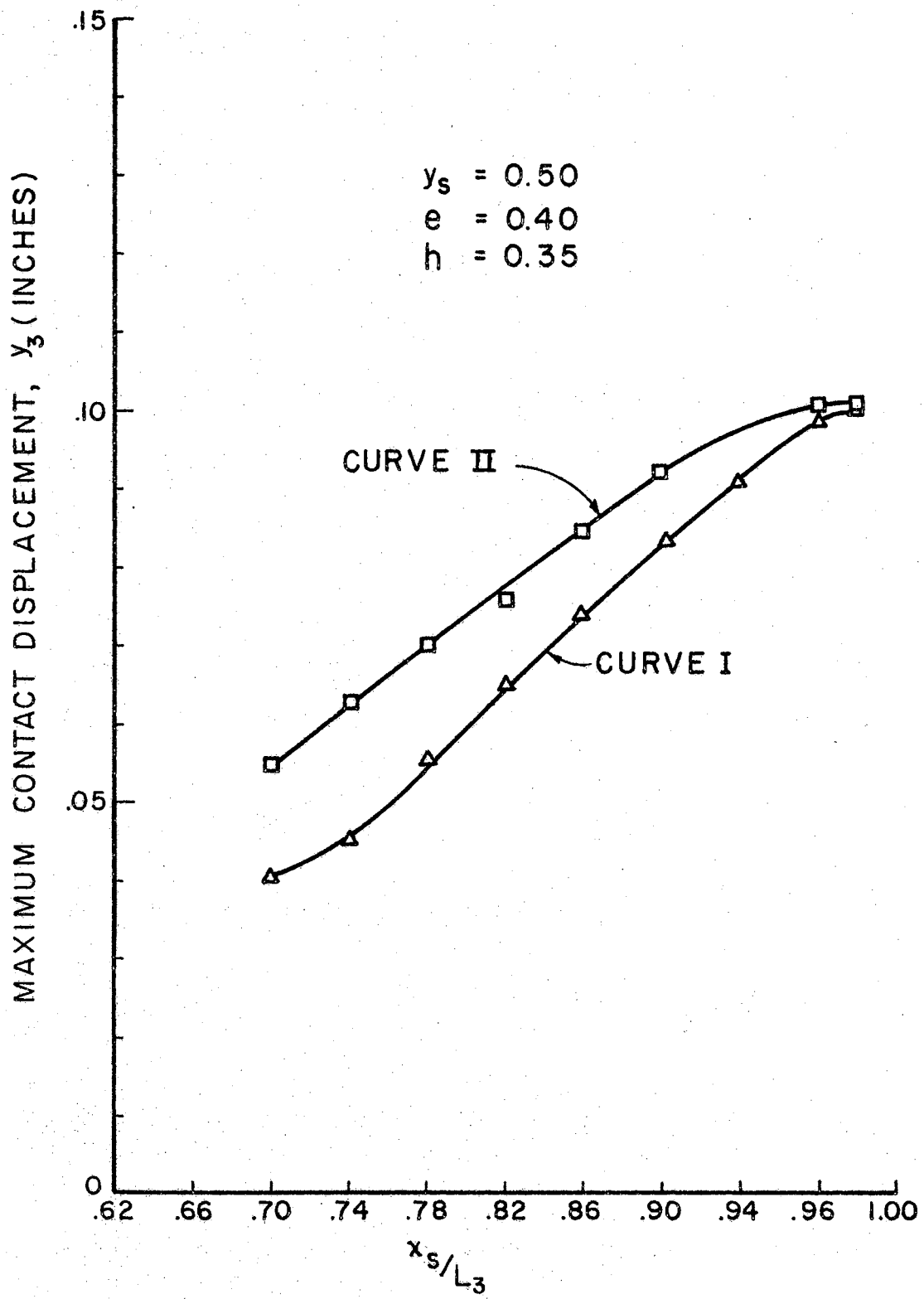


Figure 6. Maximum Contact Displacement Versus x_3/L_3

reduced when compared to a comparable value of x_3/L_3 for curve I since the stiffness is a function of both L_3 and x_3 .

As can be seen from Figure 6 the variation in the contact displacement, y_3 , indicates that the displacement, for a given contact, may be decreased by decreasing the ratio of x_3 to L_3 . This result is not surprising since as the point of contiguity is moved toward the contact support the contact stiffness increases presenting an increased deterrent to its own displacement.

The variation in x/L has an interesting consequence in regard to the complexity of the displacement response of the contact. As the ratio of x/L is adjusted the relative intensity of the specific modes in the complete contact response is adjusted also. Thus, if x/L is such that the contact separator touches the contact at a nodal point of the contact's third mode, the third mode will be absent in the displacement response of the contact at that point. Similarly, the second mode will be absent from the contact displacement response if the point of contiguity is at the node of the contact's second mode. In contrast the free end is an antinode for each mode; hence, each mode will be present at its maximum amplitude.

However, the amplitudes of the various modes are inversely proportional to the modal frequency as indicated in equation (23). Hence, the third mode will be relatively minor and it would therefore appear that a fairly simple response would result if the nodal point of the contact's second mode was selected for the point at which contact is made. At this point the third mode has a relatively small amplitude, and more important, the second mode is precluded.

Figure 7 shows a plot of the displacement versus time of the lower contact for two different ratios of x to L . Specifically, the two values of x/L shown are .98 and .78. These locations correspond approximately to the usual location of a contact button in present designs and to the node of the second mode, respectively. The graphs very definitely reflect the previous discussion. The curve for $x/L = .98$ shows definite indications of higher mode oscillations. In contrast the displacement response for a ratio of x to L of .78 appears to contain only a single mode. This is because the third mode amplitude is very small at this point. This implies that the response of the distributed parameter system emerges as a response that would be expected from a single degree of freedom system.

The behavior just described has some significant consequences. First, the reduction in x/L to, say, .78 results in a reduction in the maximum displacement of the lower contact. Secondly, the complexity of contact displacement response is significantly reduced and the response approaches that of a single degree of freedom system. Thus, if the third mode is assumed negligible, which would certainly be true in an engineering design, the possibility presents itself that a single degree of freedom, i.e., a lumped parameter model, analysis would be applicable. As is obvious from the manipulations which were requisite in Chapter III, this would provide a major simplification in the dynamic analyses of contacts in general. This simplification has the inherent and important qualification that contiguity between the contact and the contact separator occur at or close to the nodal point of the lower contact's second mode.

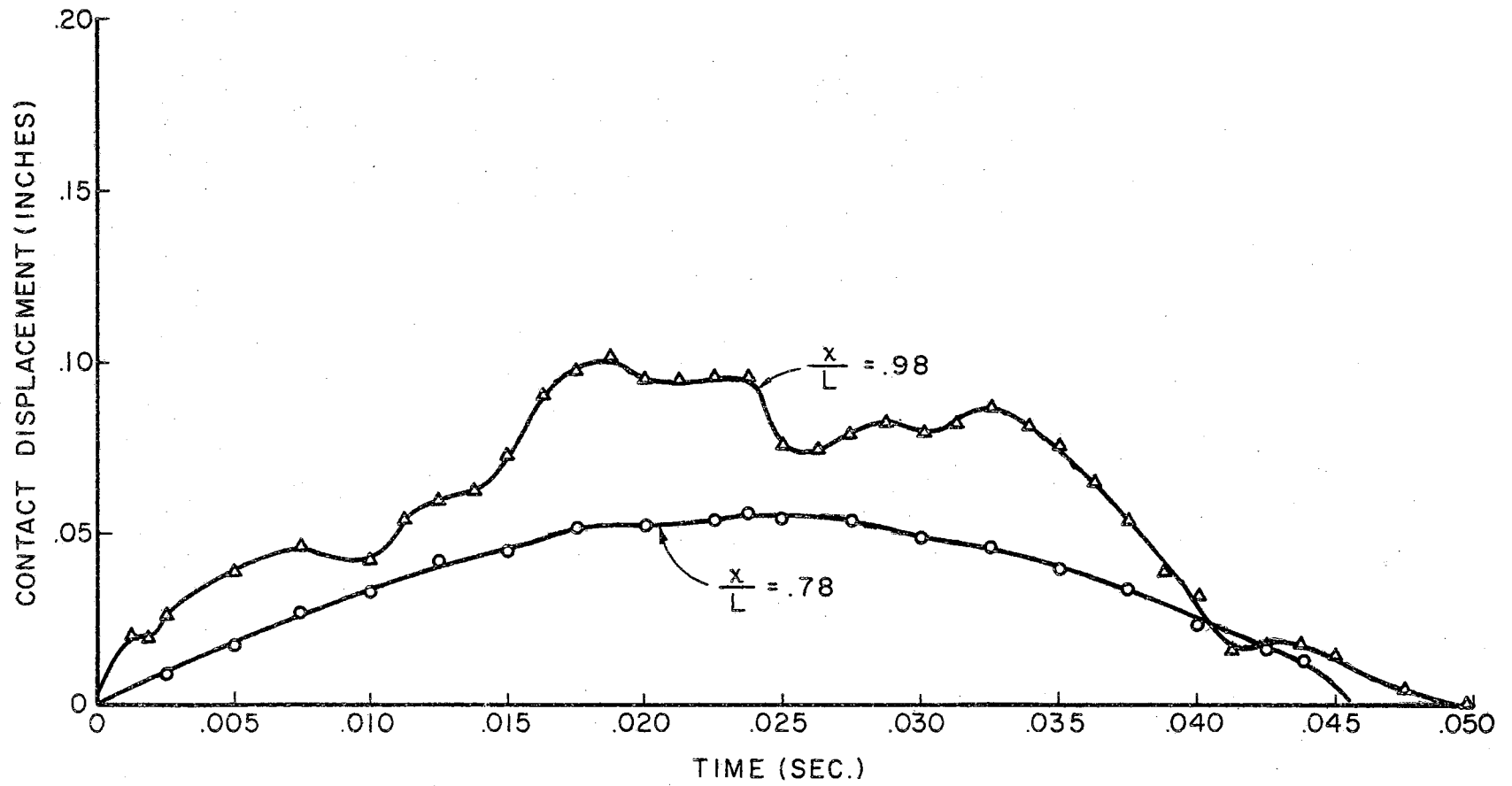


Figure 7. Contact Displacement Versus Time

The dependence of the complexity of the displacement response on the ratio of x/L has an additional ramification on the general chatter phenomenon. If contact is made at, say, x/L equal to 0.98, the second as well as third mode will be present. As such, the possibility exists that immediately subsequent to an impact some fine chatter will ensue. Fine chatter is defined as a contact bounce having a period of one of the higher modes rather than that of the fundamental mode. This was found to be evident in the analysis of Appendix E. The conclusion to be drawn is that the point at which the members are contiguous, and therefore where the normal mode functions are evaluated, is influential in determining the vibrational character of the contact chatter.

Mass Ratio

An additional parameter which is of interest is the ratio of the mass of the contact separator to that of the contact. This ratio will be denoted by the symbol R and defined by the following equation

$$R = \frac{M_2 / \sum_{j=1}^{\infty} X_{j_2}^2 (L_2/2)}{M_c / \sum_{j=1}^{\infty} X_{j_c}^2 (L_c)} = \frac{M_2^*}{M_3^*} \quad (24)$$

Due to the symmetry in the contact system the upper and lower contacts may be denoted by the subscript, c , signifying a contact. With these simplifications equation (22) becomes

$$y_c = \frac{(1+e)y_s \sum_{j=1}^{\infty} p_{jc} C_{jc} X_{jc} (L_c)}{L_a L_c (1+2R)} \sum_{j=1}^{\infty} \frac{X_{jc}^2 (L_c)}{p_{jc}} \sin p_{jc} t.$$

It has already been mentioned that it is not considered realistic to consider a variation in the mass of a contact independent of the remaining system parameters. Therefore, the total system effect of the variation will be indicated in this discussion.

Since the maximum displacement of the contact is of interest, the above equation may be evaluated at some time $t = t_m$, the time at which the maximum displacement occurs. For a given initial static displacement and x/L ratio, the terms y_s and X_j will be constants. If the mass ratio, R , is permitted to vary, the displacement of the lower contact is seen to behave as shown in Figure 8. This graph is for $x_c/L_c = 0.98$ and $x/L = 0.5$ for the contact separator with the initial static displacement of the upper contact at 0.5 inch. The plot indicates that the maximum contact displacement decreases as the mass ratio, R , increases. This, therefore, suggests that to minimize the magnitude of the lower contact displacement the mass of the contact separator be as large as possible relative to the mass of the contacts.

It should be recalled that the analysis presented in Appendix E is for repeated impacts between a cantilevered contact and a massive, flexurally rigid contact separator. As the mass of the contact separator becomes large, the analysis in Appendix E will become more valid for the top contact.

The results of the analysis in this chapter indicate that the magnitude of the lower contact separation may be reduced by decreasing the magnitude of the coefficient of restitution, the initial static displacement, the ratio of x_3 to L_3 and by increasing the mass ratio. The governing equation was also shown to be capable of generalization

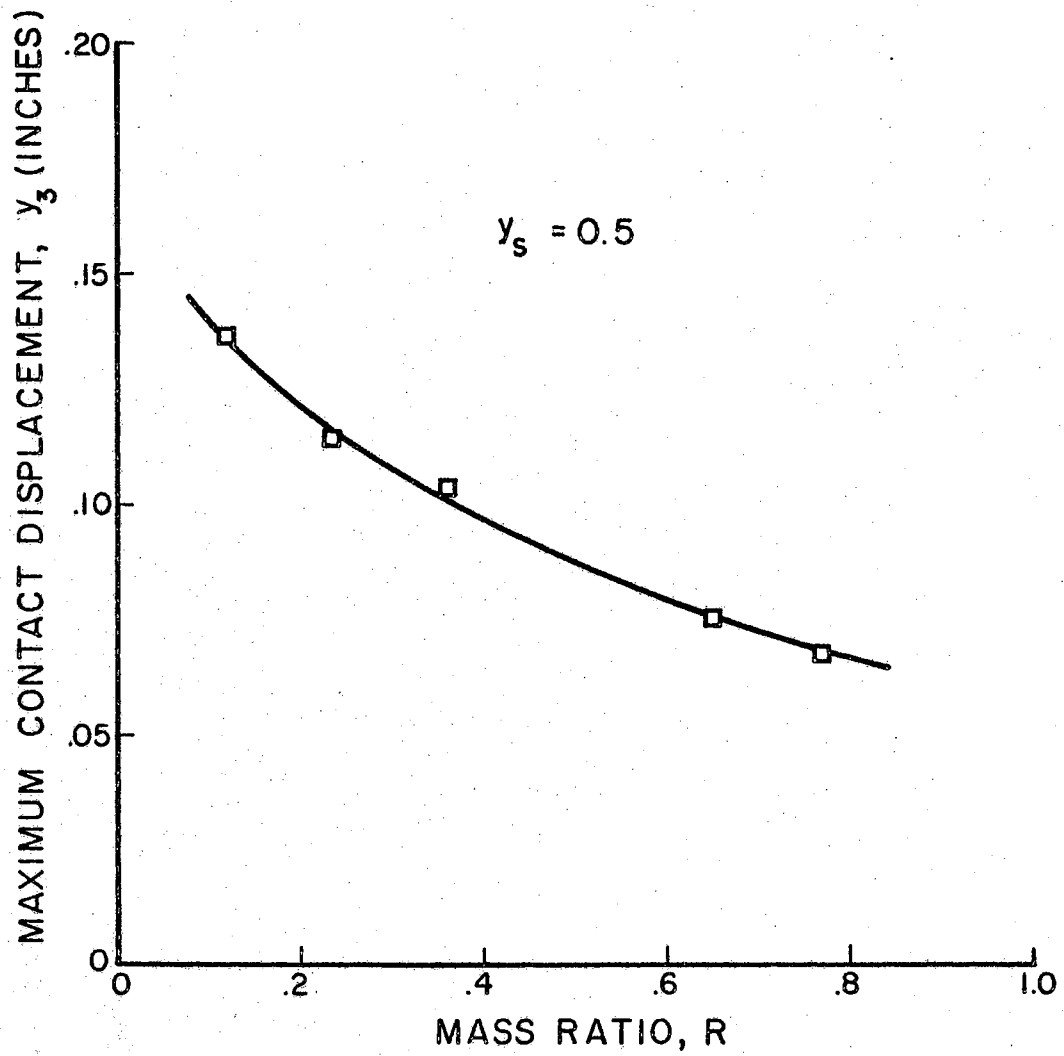


Figure 8. Maximum Contact Displacement Versus Mass Ratio

to the study of contact separation for any contact system comprised of three uniform beams. In addition, it was theoretically demonstrated that the point at which the normal mode function is evaluated will influence the complexity of the contact displacement response. If the point of contiguity between the contact and the contact separator is at the node of the contact's second mode, the displacement response will closely resemble that of a single degree-of-freedom system.

CHAPTER V

EXPERIMENTAL MODEL AND INSTRUMENTATION

In order to facilitate a study of the theory developed it was essential to build a model of the redundant contact system described in the Introduction. A large model was constructed as this would reduce the frequencies of the various oscillating members facilitating the observation of the system and minimize the influence of any instrumentation in the model on the dynamic behavior of the model.

Description of the Model

The model, devoid of its instrumentation, has been depicted schematically in Figure 1 in the Introduction. In order to minimize adjustment difficulties, as well as crowding in the model and also to make the upper and lower contact supports independent, the supports for the upper and lower contacts were placed on opposite sides of the contact separator. This arrangement is shown in the photograph in Figure 9.

As can be seen in the photograph, the supports for the cantilevered contacts were made large and massive and then attached to 24 x 24 x 1/4 inch aluminum plates in an effort to make the foundation for the entire model as rigid as practical. The entire model was then placed on 1/4-inch Isomode pads to further inhibit the introduction of extraneous motion to the model. The contact separator was held in the remaining two vertical supports as shown in Figure 10.

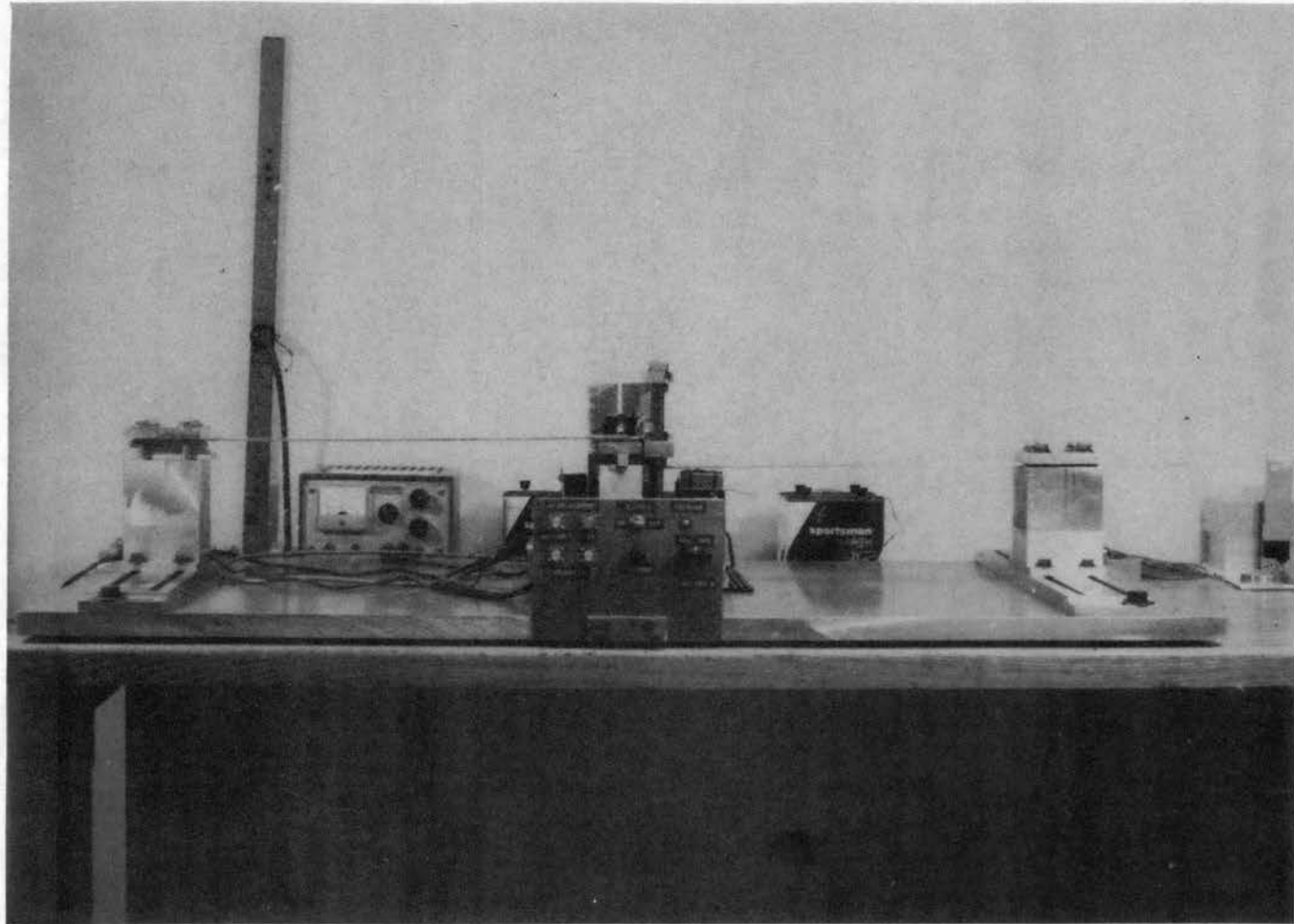


Figure 9. Experimental Model

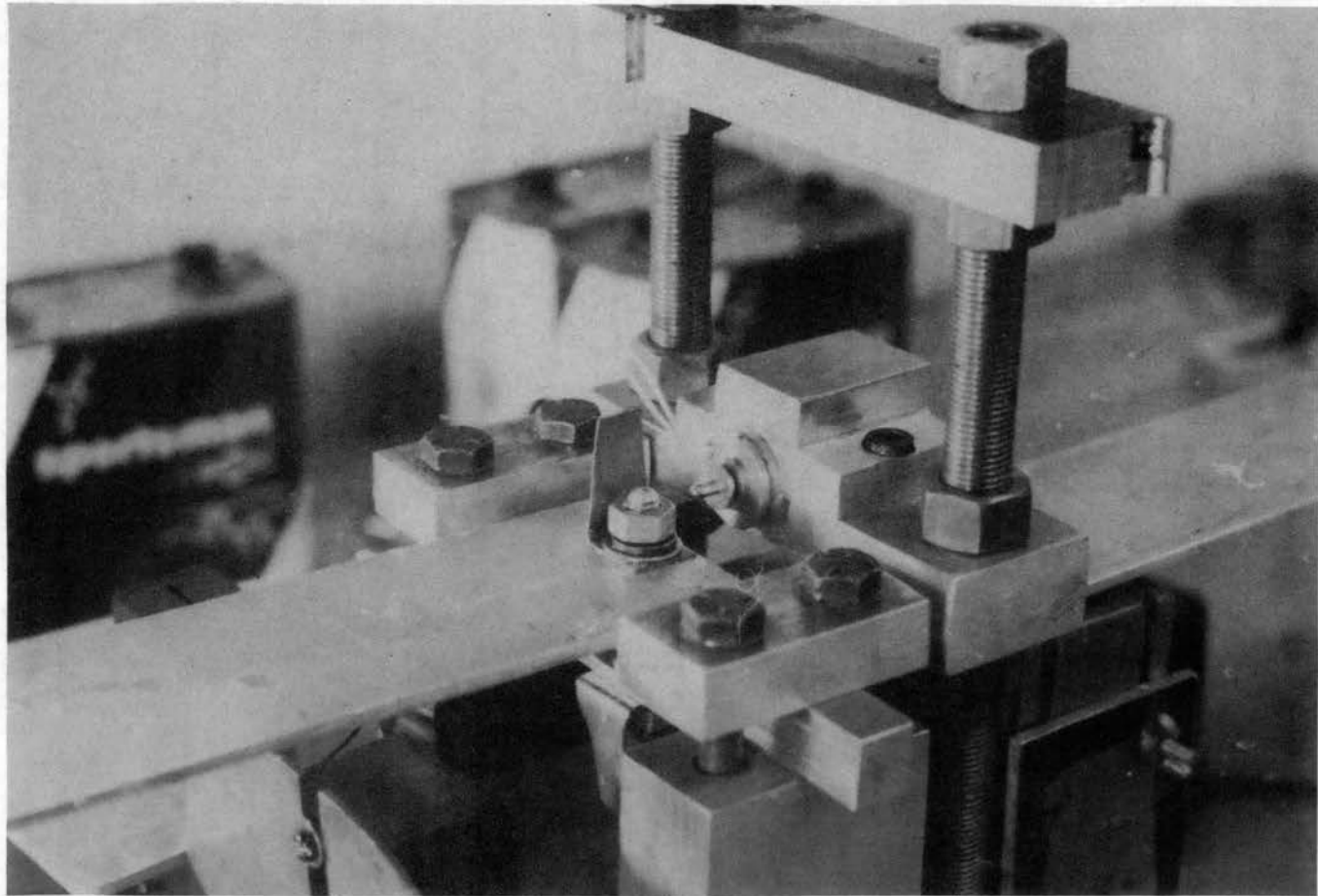


Figure 10. Solenoid and Contact Separator Clamping Arrangement

The model provided the initial static deflection of the upper contact via a solenoid placed in the solenoid holder. The solenoid holder, in turn, was supported by two vertical, 1/2 inch threaded rods as shown in Figure 10. Adjusting nuts on the top and bottom of the solenoid holder permitted a one degree of freedom variation in the location of the solenoid with respect to the contact separator.

Both the contacts and the contact separator were constructed of aluminum. The contacts were 19 inches long, 2 inches wide and 1/8 inch thick. Each of the contacts was provided with hemispherical contact buttons, also of aluminum, and located near the free end of the contact.

The contact separators were all 2 and 1/2 inches long and 1/2 inch wide; however, the thickness of the contact separator was permitted to vary. Contact separator thicknesses of .125, .250, .350, .500 and .750 inches were employed in the model.

Instrumentation

In order to measure the contact displacements a transducer having fast response time, good sensitivity and a high signal to noise ratio was needed. In addition, it was highly desirable that there be a minimum of reflected inertia from the transducer to the contact. All the aforementioned characteristics implied an optical system and for this reason a photocell arrangement was employed. The photocells were photovoltaic, silicon cells. The light incident on the photocells was interrupted by a metallic shade attached to the contacts as shown in Figure 11. As the contact was displaced, the position of the shade relative to the stationary photocell and light source was changed thus varying the intensity of the

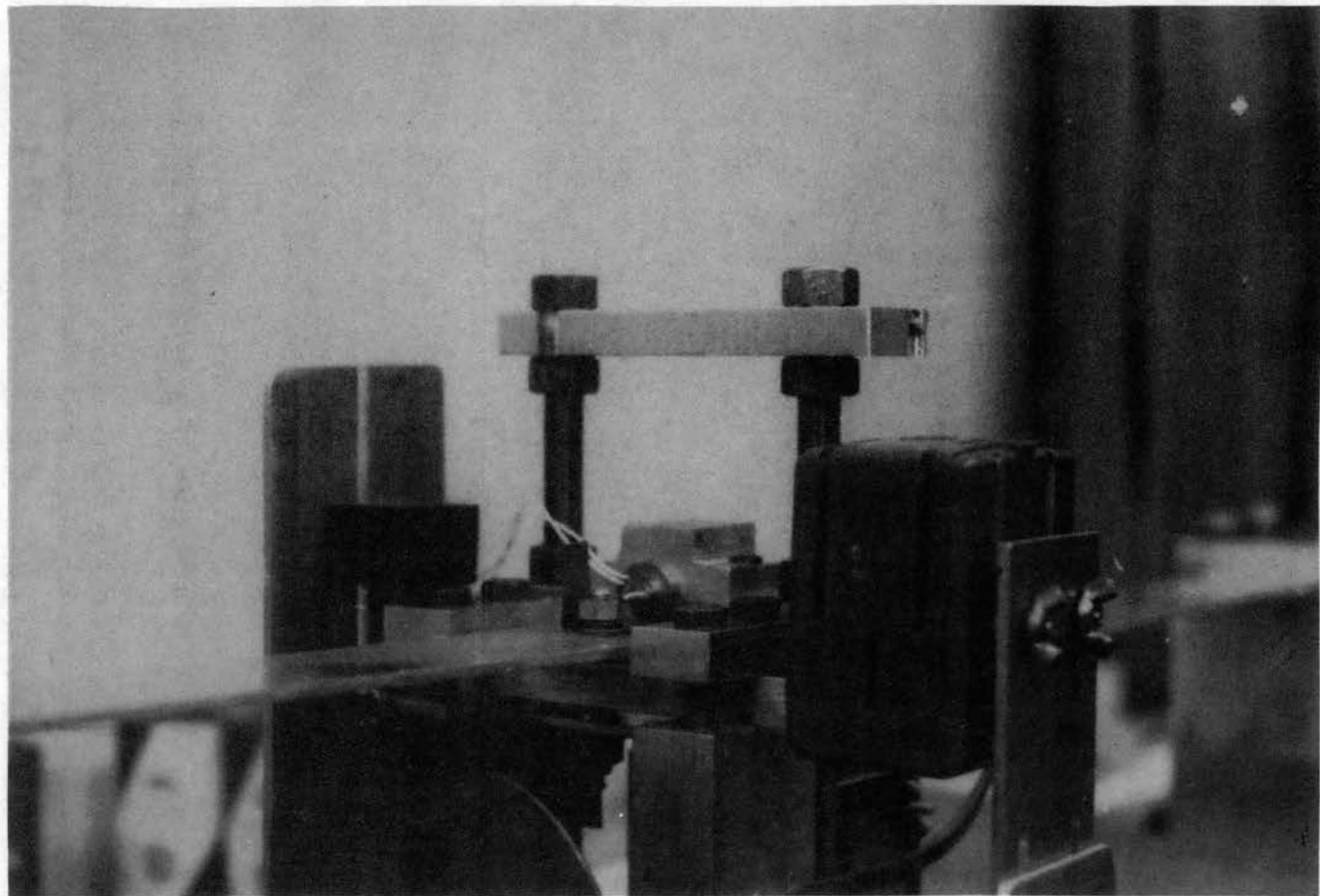


Figure 11. Photocell and Light Source Arrangement

light incident on the photocell and yielding a displacement sensitive system.

Contact velocity measurements were initially attempted by differentiating the photocell signal but the requisite intermediate instrumentation had deleterious effects on the signal and this approach was abandoned. Instead an independent velocity transducer was utilized. The velocity transducer consisted of a high coercive force permanent magnet core moving concentrically within a shielded coil. Voltages are then generated, without external excitation, which vary linearly with the velocity attained by the core.

A dual beam cathode ray oscilloscope was used for readout purposes on all the instrumentation. A block diagram of the instrumentation and the electrical interconnections is shown in Figure 12. A photograph of the complete experimental assembly is shown in Figure 13.

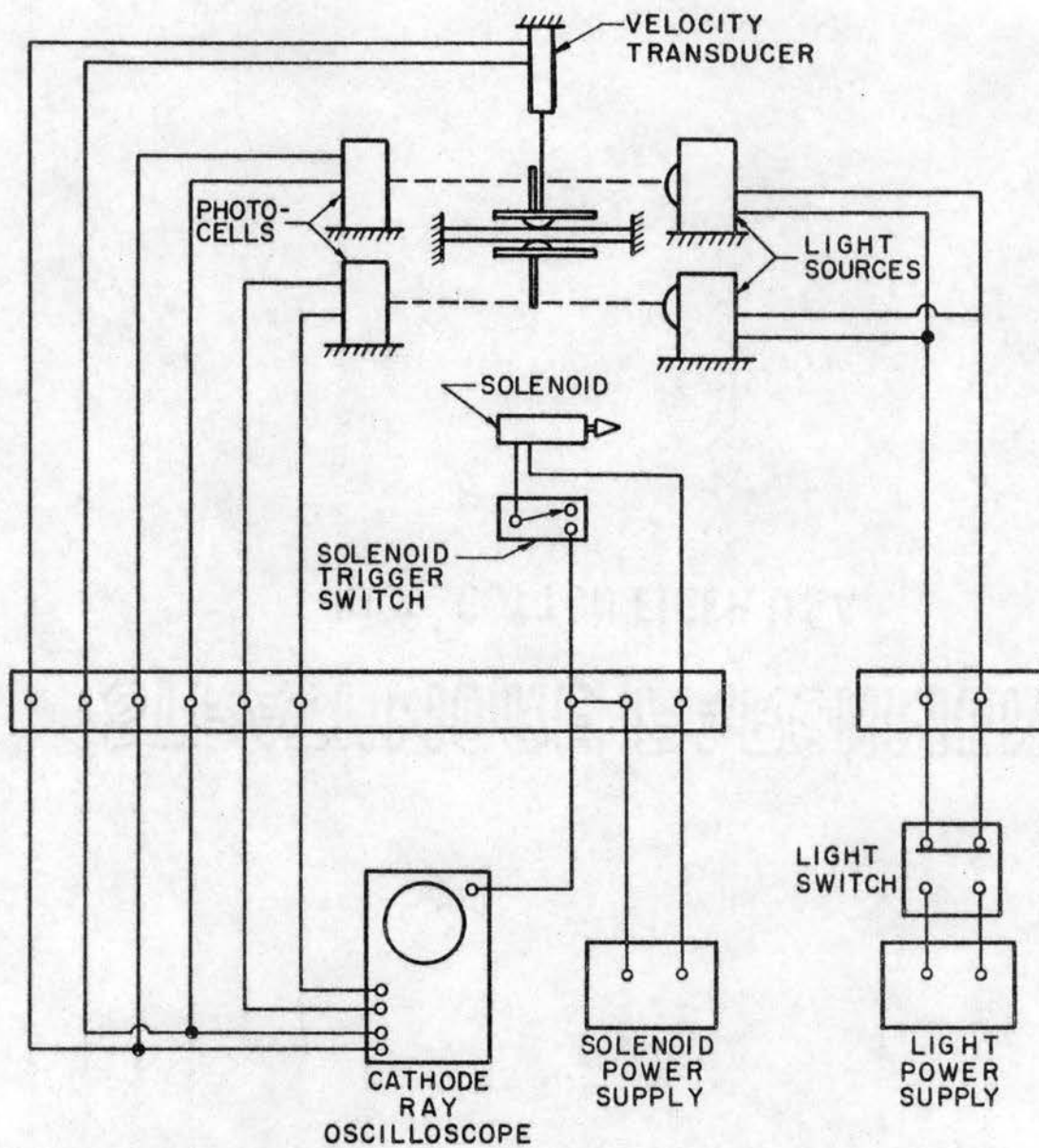


Figure 12. Block Diagram of the Instrumentation

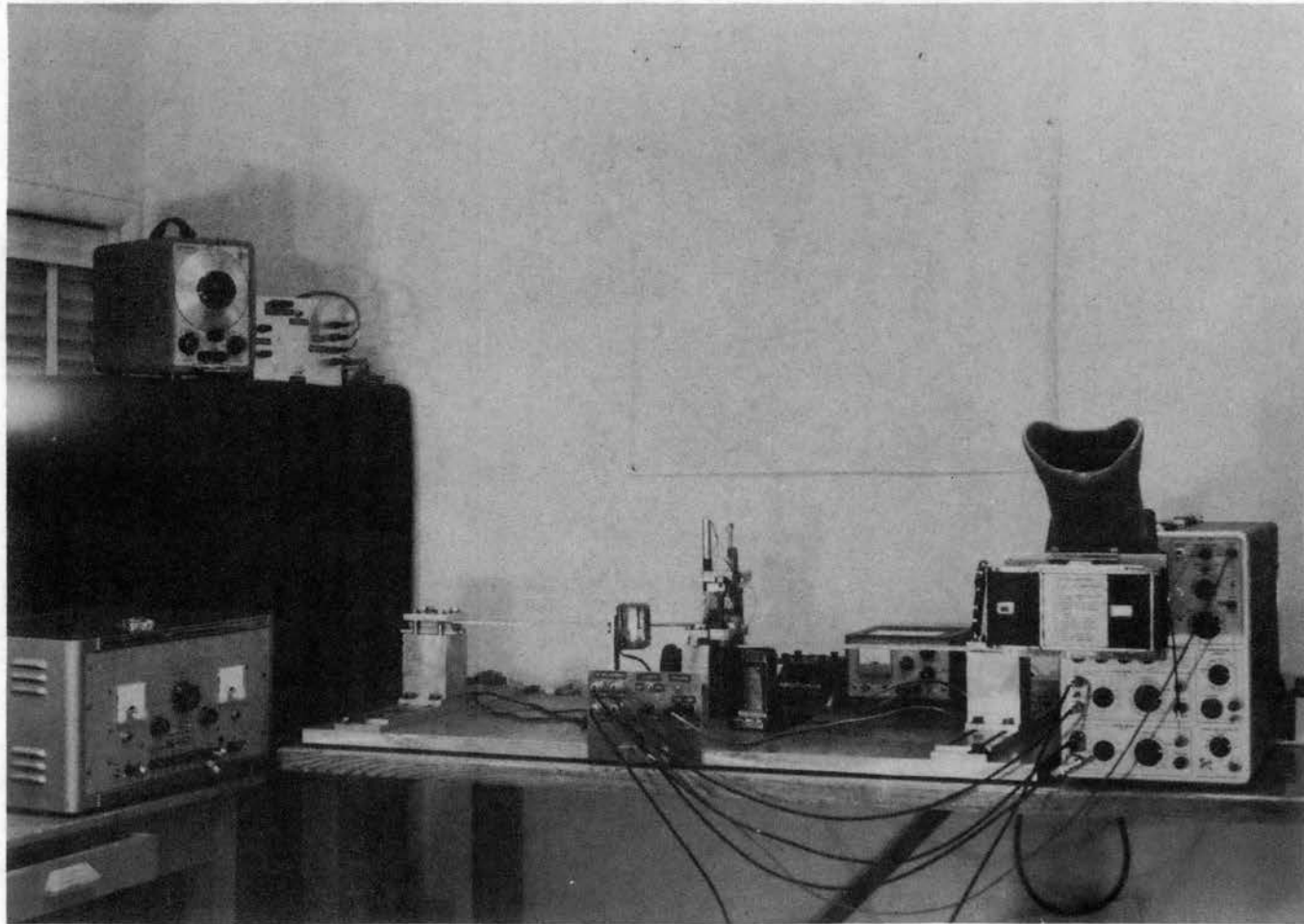


Figure 13. Experimental Model With Instrumentation

CHAPTER VI

EXPERIMENTAL PROCEDURE AND RESULTS

The essential goal of the experimental portion of this study was to substantiate the validity of the trends indicated by the proposed mathematical model for the behavior of the system to be studied. The laboratory effort also yielded a more intimate understanding and appreciation for the physical parameters of the system and the general validity of the theoretical assumptions made in the analysis. It also provided an invaluable stimulus towards the final analysis.

Prior to initiating the investigation of the model and its behavior, the calibrations of the various components of the instrumentation were verified. The displacement transducers were calibrated during each experimental run since the position of the photocell relative to the shade, on the contact, and the light source were critical.

The velocity transducers were calibrated with an MB-C11 vibration exciter. The transducer and the associated instrumentation for this calibration are shown in the photograph in Figure 14. Displacement and frequency readings from the vibration exciter were compared with the voltage output of the velocity transducer.

Model Parameters

The model parameters which were studied were the contact and contact separator natural frequencies and the coefficient of restitution.

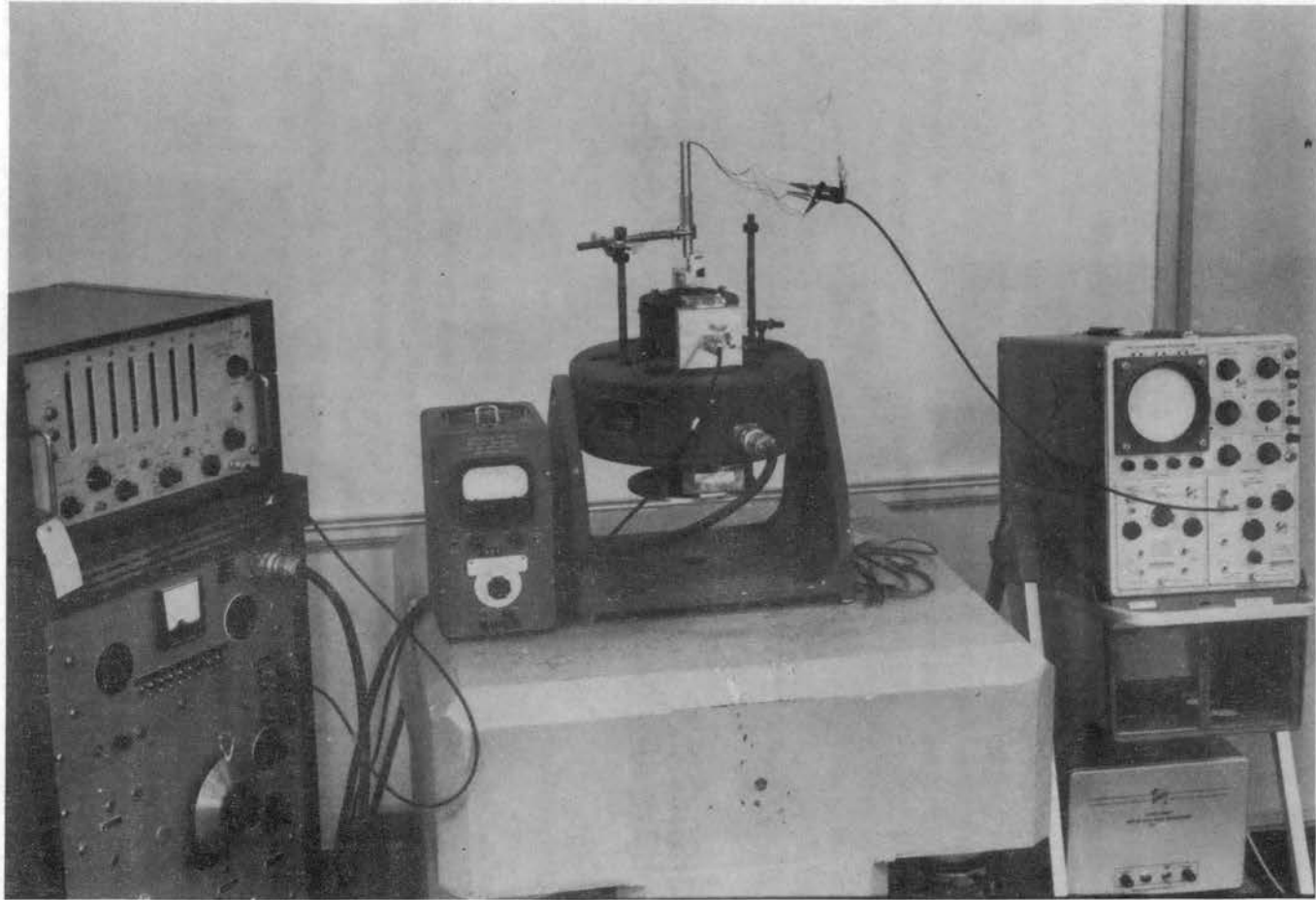


Figure 14. Velocity Transducer Calibration Arrangement

An experimental check of the natural frequency of each of the contacts as well as the contact separator was made with the MB-C10E vibration exciter. Care was taken to support the vibratory members as they were supported in the experimental model.

A verification of the natural frequency generally will serve as a check of several of the hypotheses made in the theoretical derivations. First, it can yield an indication of how well the assumed boundary conditions are met. In the derivations of the vibrational response equations it was assumed that these boundary conditions were fulfilled. This requirement is, unfortunately, rarely, if ever, met in an actual physical system. Of the orthodox beam boundary conditions, the clamped end condition is perhaps the most difficult to achieve. A deviation from an ideal clamped condition would permit additional deflection in the beam resulting in an apparently longer and softer member. The experimental natural frequency of a beam whose clamped boundary condition is less than ideal would therefore exhibit a natural frequency which is less than that predicted by theory. A second deviation in the natural frequencies is possible due to the neglect, in the Bernoulli-Euler beam equation, of shear and rotatory inertia effects. These effects are normally significant in short stubby beams, that is, members in which the length is not significantly greater than the lateral dimensions. A beam in which the shear and rotatory inertia effects are not negligible will also exhibit a natural frequency whose magnitude is less than that predicted by the Bernoulli-Euler theory.

To investigate the natural frequencies of the contacts, the contacts and the contact supports were removed from the experimental model and

mounted on the MB-C10E vibration exciter. This arrangement is shown in the photograph in Figure 15. A resonance search was made to ascertain the first four vibrational modes of each of the contacts. Two visual indicators were used to determine the frequency at which the contact exhibited a resonant condition. Visual observation was made with the aid of a Chadwick-Helmuth Strobex system. This is a strobelight system in which the phase between the vibration exciter and the strobelight may be varied uniformly and continuously through 360 degrees. With this capability it is possible to observe the contact displacement in slow motion. In addition, the sand pattern technique was employed. In this technique, a fine grain sand is sprinkled on the entire contact prior to excitation or during excitation of the contact. As a resonant condition is achieved the sand is thrown off the contact at any displacement antinodes while simultaneously being accumulated at the nodes. When a resonant frequency was achieved an amazingly sharp sand pattern, consisting of stationary, transverse rows of sand at each nodal line, was observed on the contact. The sand patterns indicating the nodal regions for the second through fourth mode of the contact are shown in the photographs in Figures 16 through 18. As can be seen from the photographs the sand patterns indicate sharply defined nodal regions. In addition, the sand patterns are normal to the longitudinal axis of the contact. This would connote that little or no torsional mode is generated in the contact beams. The resonant frequency was read on a digital frequency meter.

The theoretical contact natural frequencies were calculated from the eigenvalues of the cantilever beam frequency equation, which is

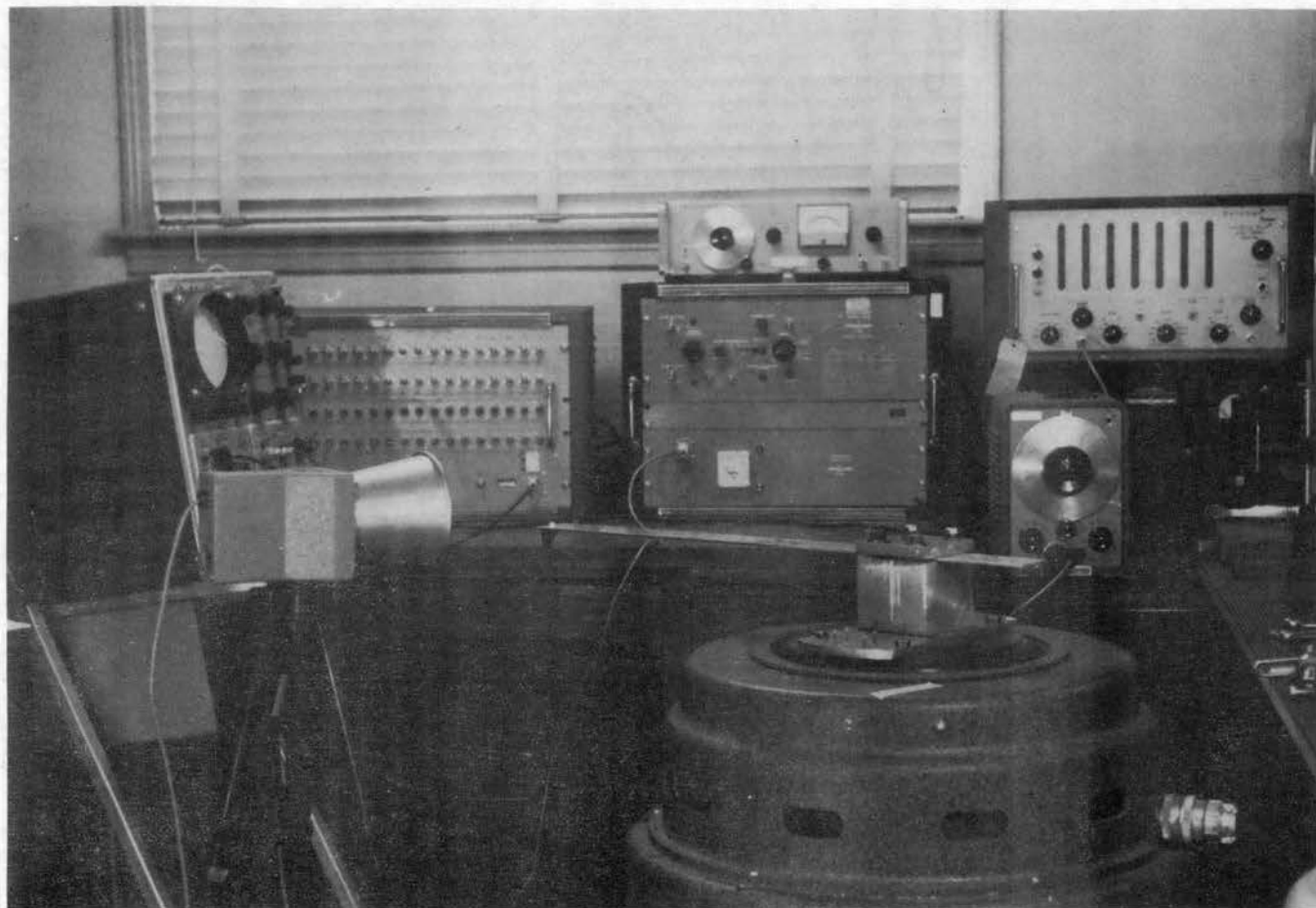


Figure 15. Experimental Arrangement for Finding the Natural Frequencies of the Contacts

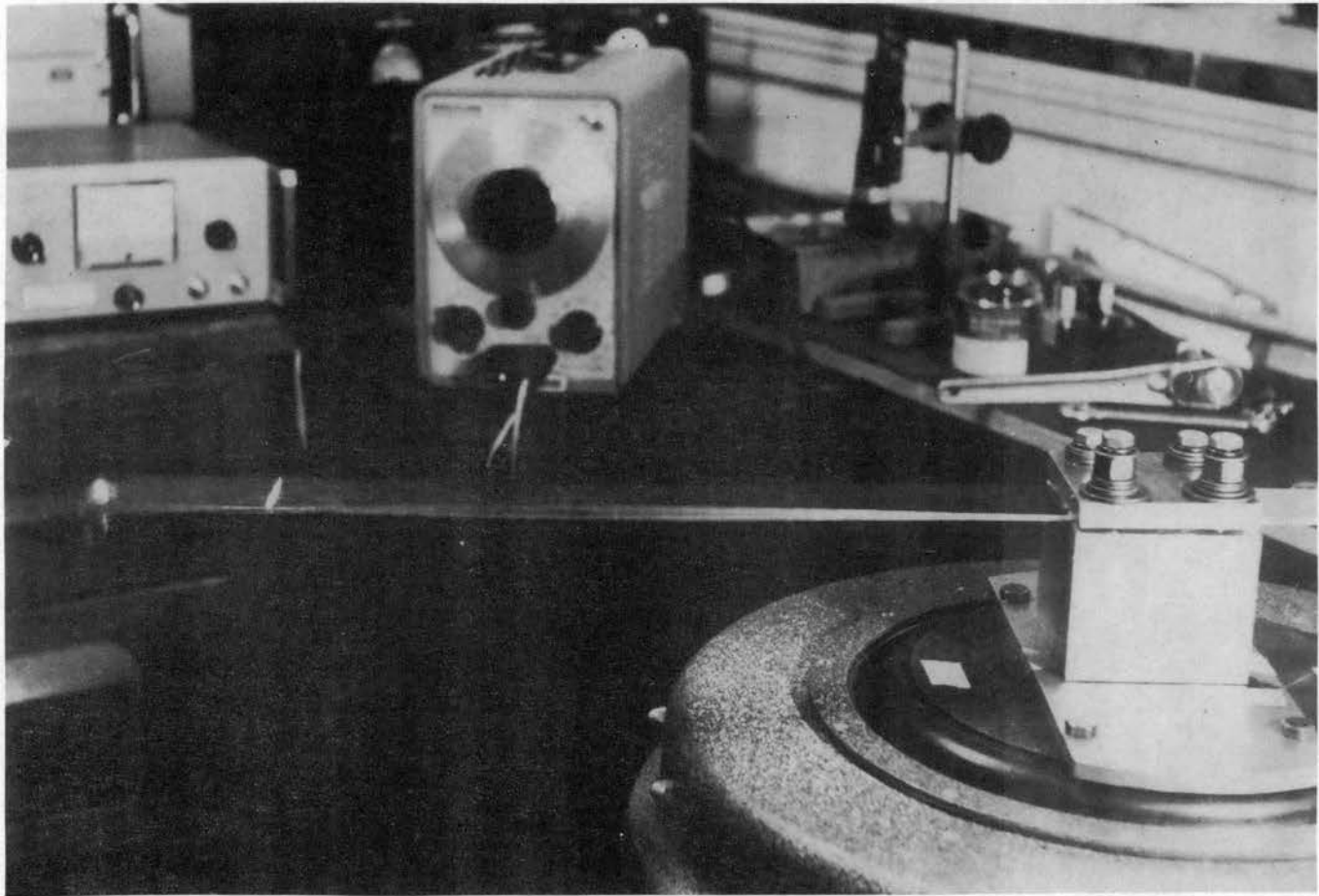


Figure 16. Sand Pattern for the Second Mode of the Contact

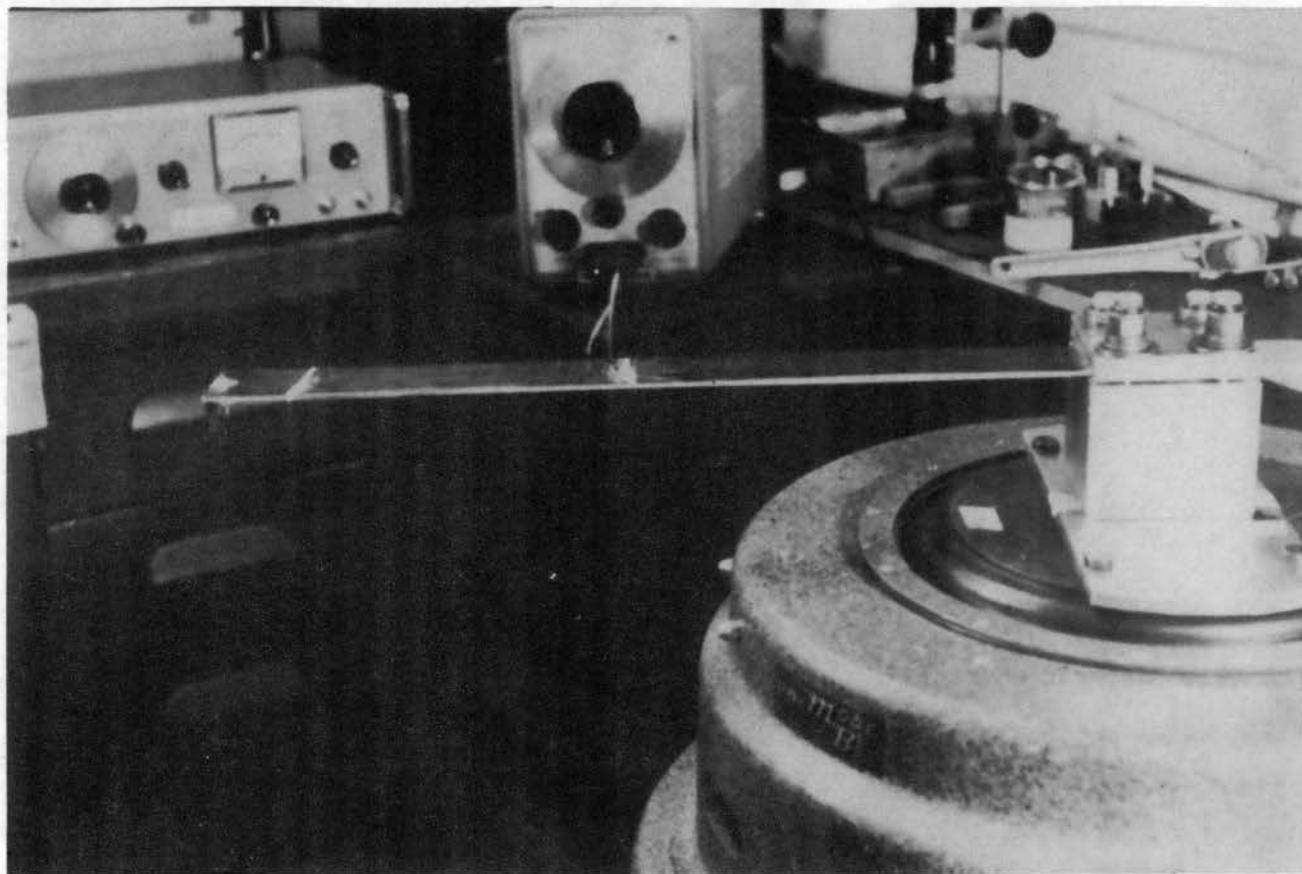


Figure 17. Sand Pattern for the Third Mode of the Contact

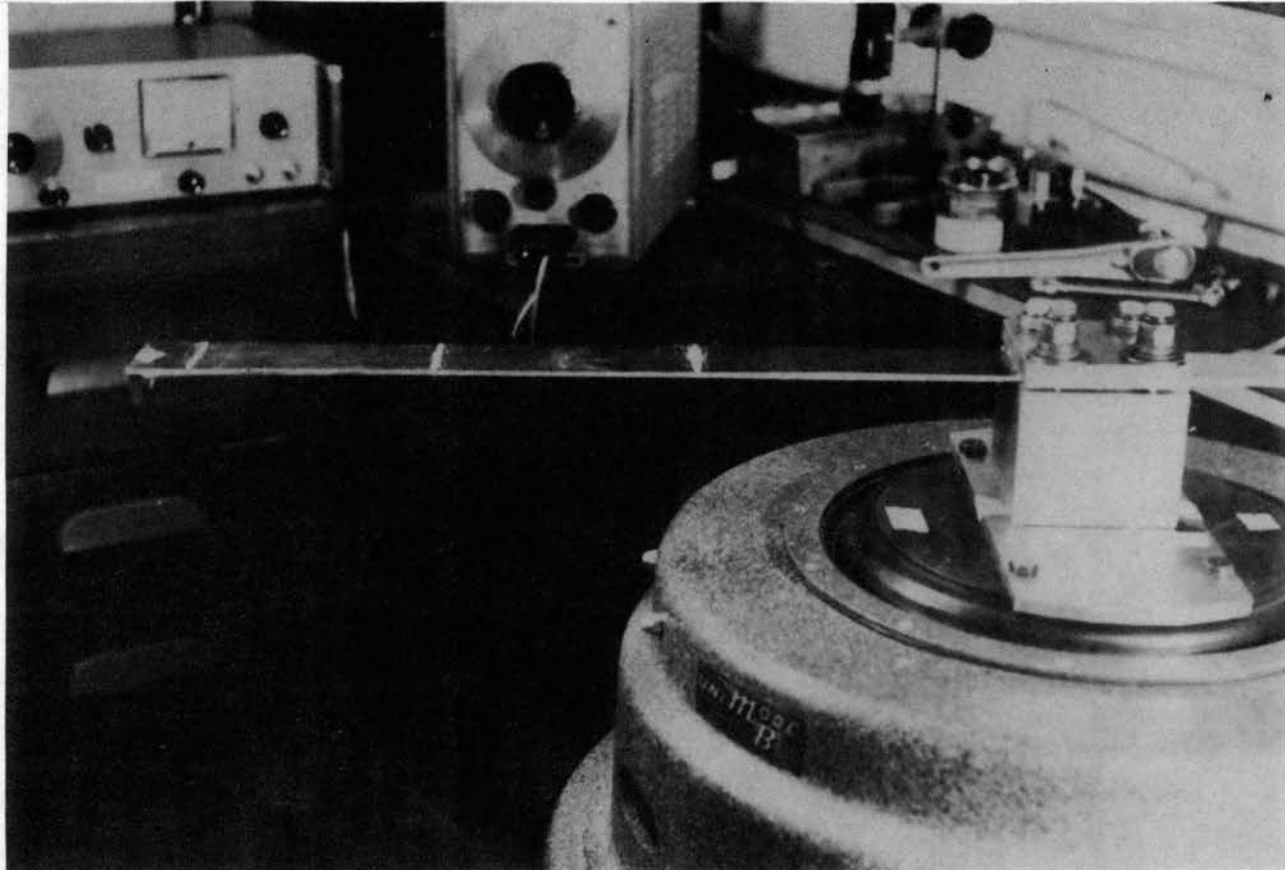


Figure 18. Sand Pattern for the Fourth Mode of the Contact

$$\text{Cosh } k_j L \text{ Cos } k_j L = -1,$$

where $k_j = (p_j/a)^{\frac{1}{2}}$. Both the experimental and theoretical values, in cycles per second, are given in Table I and are in excellent agreement. It should be noted that the rigidity of the contact supports is much greater than the stiffness of the contacts and also that the length to depth ratio of the contact is large. With such a configuration it would be expected that the boundary conditions would be satisfied and that shear and rotatory inertia effects could be neglected. The close agreement between the experimental and theoretical contact natural frequencies certainly support this statement.

TABLE I
THEORETICAL AND EXPERIMENTAL CONTACT
NATURAL FREQUENCIES

Upper Contact		
Mode	Theoretical (cps.)	Experimental (cps.)
1	10.6	10.3
2	66.5	65.0
3	187.0	180.0
4	366.0	360.0
Lower Contact		
Mode	Theoretical (cps.)	Experimental (cps.)
1	10.6	10.6
2	66.5	67.0
3	187.0	186.0
4	366.0	371.0

The natural frequency of the contact separator was also investigated with the MB-C10E vibration exciter. The procedure was essentially the same as with the contacts except that, due to the small displacements exhibited by the contact separator, accelerometers were used to indicate when the resonant condition was reached. In this case two accelerometers were needed. One accelerometer was mounted on the vibration exciter head; the other accelerometer was attached to the contact separator with dental cement. Both of the accelerometer outputs were then simultaneously monitored on a dual beam, cathode ray oscilloscope as the exciting frequency was varied. When the resonant frequency of the separator was reached the output of the accelerometer on the separator indicated a significant increase while the accelerometer on the exciter remained relatively unchanged. The experimental values of the contact separator natural frequency was read on a digital frequency meter.

The theoretical natural frequency of the contact separator was calculated from the eigenvalues of the clamped-clamped beam frequency equation, which is

$$\cos k_j L \cosh k_j L = 1.$$

The theoretical and experimental values are listed in Table II.

In contrast with the contacts the theoretical and experimental values for the natural frequency of the contact separator are not in good agreement. Here two of the original assumptions must be recollected. First, it was assumed that the contact separator motion could be represented by Bernoulli-Euler beam equation. Secondly, it was hypothesized that the ideal clamped boundary conditions were fully satisfied.

TABLE II
THEORETICAL AND EXPERIMENTAL CONTACT
SEPARATOR NATURAL FREQUENCY

Separator Thickness(in.)	Theoretical (cps.)	Experimental (cps.)
0.125	4050.0	2,000.0
0.250	8100.0	4,000.0
0.350	11,310.0	5,000.0
0.500	16,200.0	6,250.0
0.750	24,300.0	11,100.0

In all the above cases the experimental values are lower than those predicted by the Bernoulli-Euler beam theory. This would indicate that either some elasticity existed in the contact separator supports or that Timoshenko beam behavior is present. A third alternative is that of non-ideal boundary conditions accompanied by shear and rotatory inertia effects in the contact separator. It should also be noted that the discrepancy increases as the contact separator thickness, d , increases. This is to be expected since as d increases the stiffness of the separator becomes more comparable to that of the supports and the d/L_2 ratio increases resulting in a greater susceptibility to shear and rotatory inertia effects. It is probable that both phenomenon exist, but the relative contributions of the individual effects on the magnitude of the discrepancy was not investigated. Instead, a correction factor was applied to the contact separator length to account for the combined effects.

From Table II, it can be seen that each of the separators exhibited a resonance which was lower than theoretically predicted. That is, it behaved as a member having lower stiffness, i.e., a beam of greater length. On this basis the correction factor was derived from the eigenvalues of the frequency equation for the clamped-clamped beam. These eigenvalues are determined solely by the boundary conditions on the beam and are invariant with the beam length. Thus, for any ideal clamped-clamped beam obeying the Bernoulli-Euler beam equation the following equality is valid,

$$k^2 L^2 = \frac{pL^2}{a} = 22.4$$

For the contact separators used in this study,

$$k^2 = 1.72 \times 10^{-5} p/d.$$

The symbol, L_c will be used to denote the length of a theoretically equivalent beam which obeys the idealized hypotheses of the mathematical model. The equivalent length may then be determined from the equation,

$$L_c^2 = (1.3 \times 10^6) \frac{d}{p}.$$

The values for d , p , and the resultant equivalent length L_c are listed in Table III.

TABLE III

EQUIVALENT LENGTH OF THE CONTACT SEPARATORS

<u>d(in.)</u>	<u>p(rad./sec.)</u>	<u>L_c(in.)</u>
0.125	12,560.0	3.60
0.250	25,120.0	3.60
0.350	31,400.0	3.81
0.500	39,250.0	4.07
0.750	70,000.0	4.15

Coefficient of Restitution

The coefficient of restitution was originally defined by Newton as the ratio of the rebound and impact velocities. The magnitude of the ratio was assumed to be determined solely by the particular materials involved in the collision.

More recent studies of impact phenomena indicate that more collision parameters are definitely involved in the determination of the magnitude of the coefficient of restitution than just the materials. However, no mathematical relationship is preferred for the determination of the magnitude of the coefficient. Consequently, the only alternative is to determine the magnitude of the coefficient of restitution experimentally, for the collision under study.

For this reason it was deemed advisable to investigate any variation in the magnitude of the coefficient of restitution with the two major experimental variables, the contact separator thickness and the initial static deflection of the upper contact. The variation of these two parameters might alternatively be considered as changes in the ratio of the masses and impact velocities, respectively.

The experimental values of the coefficient of restitution were obtained with the aid of a velocity transducer attached to the upper contact. The velocity transducer output was viewed on the cathode ray oscilloscope and a sample trace of this data is shown in Figure 19. The time base is from left to right in the photograph. The velocity of the tip of the contact will undergo a reversal in sign when it impacts on the contact separator. Therefore, the impact point will result in a vertical step discontinuity in the velocity trace as the velocity changes from a

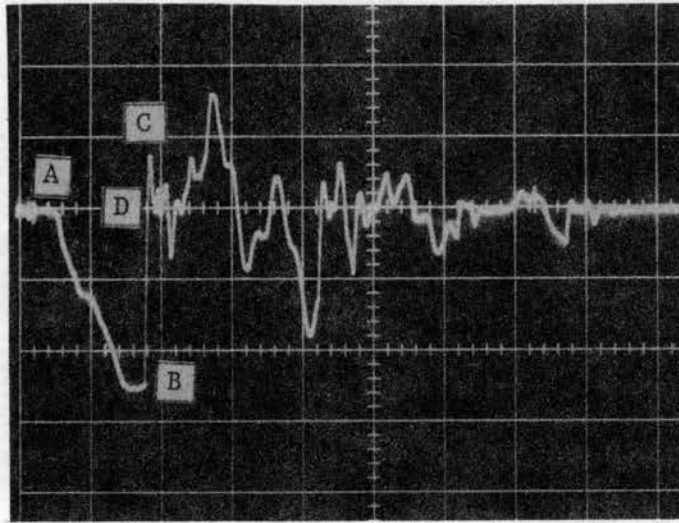


Figure 19. Velocity Transducer Response

negative to a positive value. In Figure 19, the velocity from release of the contact until impact occurs is represented by that portion of the trace from points A to B. The coefficient of restitution was then taken to be the ratio of ordinate CD to ordinate DB, i.e., the ratios of the rebound velocity to the impact velocity.

To determine if the coefficient of restitution was a function of the impact velocity the magnitude of the coefficient was determined for several values of the initial static deflection of the upper contact. These impacts were all made on the same contact separator and a plot of the coefficient of restitution versus impact velocity is shown in Figure 20.

The plot indicates a slight dependence of the coefficient of restitution on the impact velocity as indicated by a decrease in the magnitude of the coefficient with increasing impact velocities. The plot also

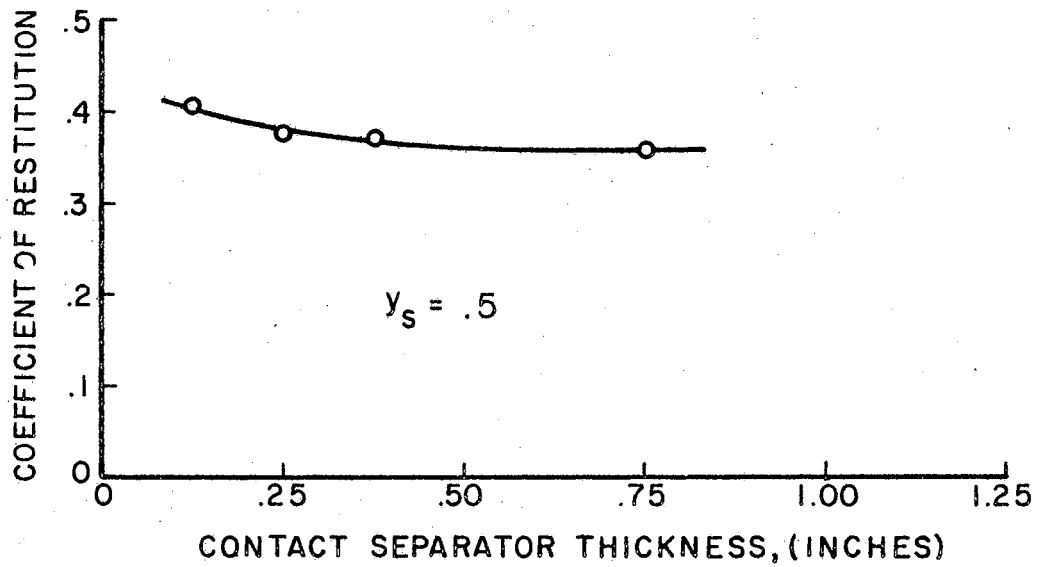
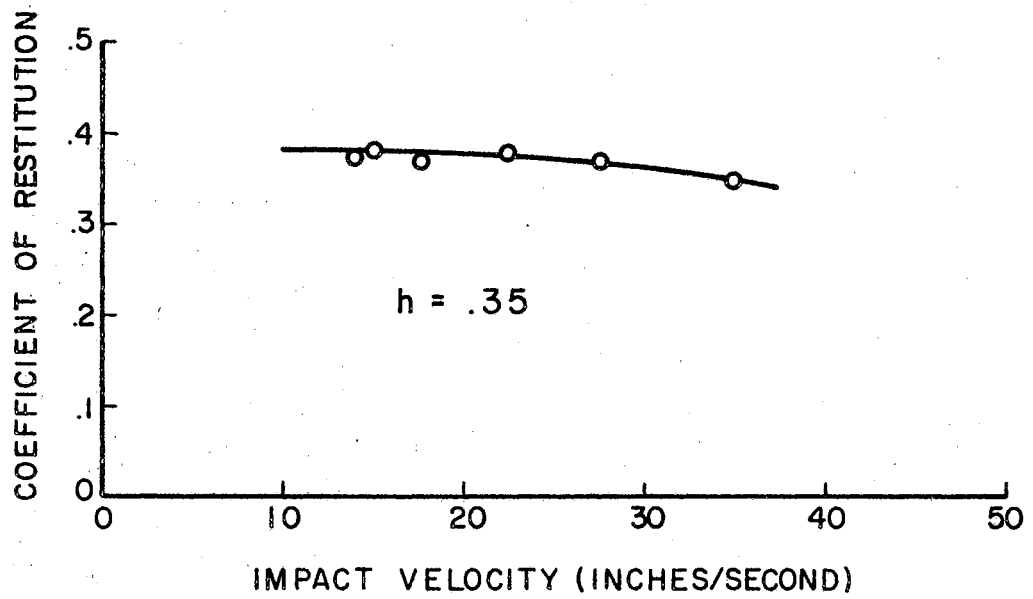


Figure 20. Coefficient of Restitution Parameters

implies therefore that an increased impact velocity would be a means of reducing the coefficient of restitution. Though a decreasing coefficient of restitution is desirable in that it implies a more inefficient collision, the decrease in efficiency is small in comparison with the corresponding increase in impact velocity and its grossly deleterious effects on the displacement of the lower contact.

To investigate the possibility of a variation in the coefficient of restitution with contact separator thickness, the coefficient was measured for the impact of the upper contact on separators of several thicknesses. The initial static displacement was held constant for all the various separator thicknesses to preclude the influence of the impact velocity dependence from entering the results. The results of this investigation are shown in Figure 20 which contains a graph depicting the variation of coefficient of restitution with the thickness of the contact separator. This plot is for an initial static deflection of 0.5 inch of the upper contact and shows a decrease in the magnitude of the coefficient of restitution with the separator thickness, d . The magnitude appears to become stationary as h increases.

The data plotted in these curves show a slight dependence of the coefficient of restitution on separator thickness as well as impact velocity. It should be pointed out that in these experiments the vibratory members, the hemispherical contact shapes and materials were invariant. Any specification of the coefficient of restitution must be qualified by specifying the bodies, materials and velocities involved in the collision under discussion.

If the adjustments described in the preceding discussion on the contact separator natural frequency and the coefficient of restitution are incorporated into the mathematical model, the predicted maximum lower contact displacements will be as shown in Figure 21. If the curves in this figure are compared with the curves plotted in Figure 5, it can be seen that there is a decrease in the maximum displacement of the lower contact.

Test Procedure

Subsequent to properly mounting the appropriate members in the experimental model the test procedure was as follows:

1. Adjust the solenoid to obtain the desired initial static displacement of the upper contact.
2. Adjust the illuminator power supply, oscilloscope sweep and sensitivities.
3. Note the initial displacement, separator thickness and oscilloscope settings.
4. Calibrate the photocells for displacement using shims of known thickness between the contact and the contact separator.
5. Raise the upper contact and rest it on the extended solenoid plunger.
6. Connect the solenoid d.c. power supply to oscilloscope external trigger input.
7. Trigger the solenoid and oscilloscope.
8. Photograph the oscilloscope traces.

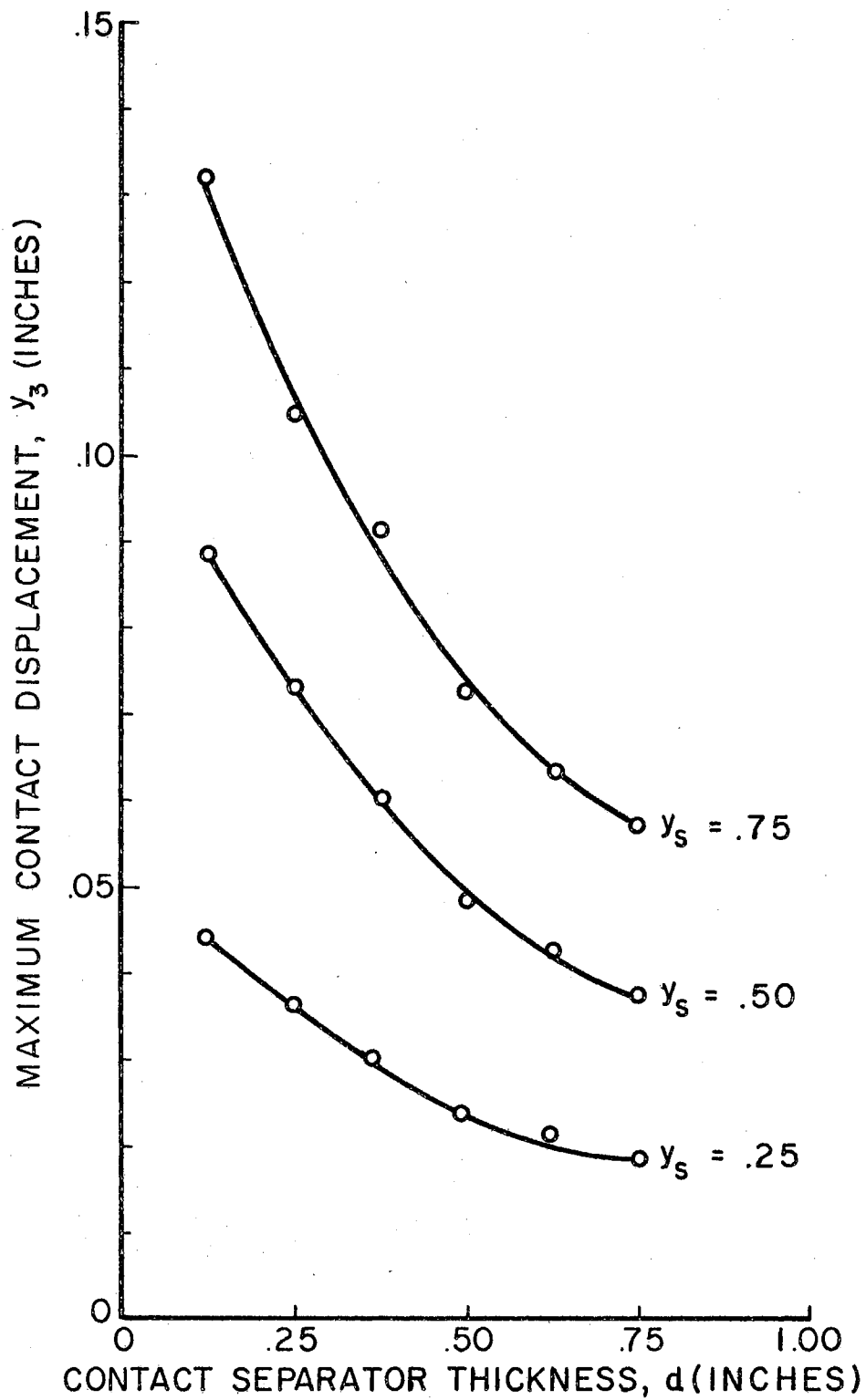


Figure 21. Corrected Theoretical Maximum Contact Displacement Versus Contact Separator Thickness

A typical pair of traces for the upper and lower contact displacement is shown in the photograph in Figure 22. The trace displays the initial impact as well as subsequent collisions of the contacts and the contact separator. The displacement response shows very definite signs of higher mode response in the contacts.

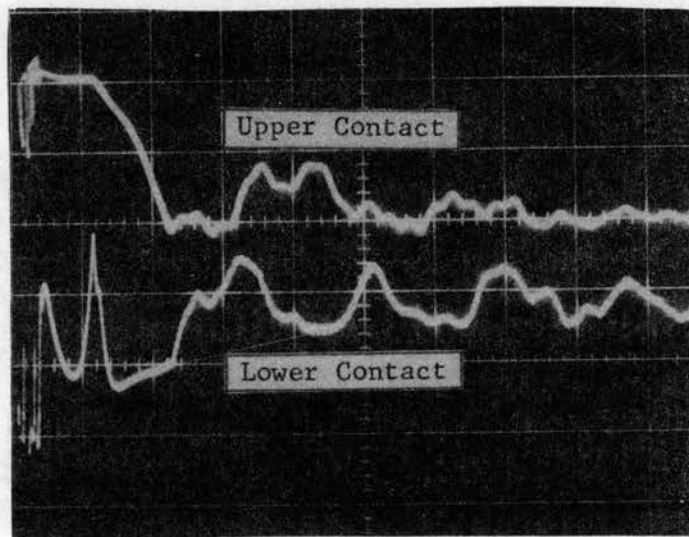


Figure 22. Contact Displacement Response

A comparison of the predicted and the experimental maximum displacements of the lower contact is shown in Figure 23. The plot is for an initial static displacement of 0.5 inches and a coefficient of restitution of 0.375.

The trends indicated by the experimental data and the theoretical values predicted by the mathematical model are in good agreement. However, there is a discrepancy in the magnitudes of the maximum values for the displacement of the lower contact. In all cases the theoretical predictions are greater than the corresponding experimental values. The experimental data points shown are single values in that only one value

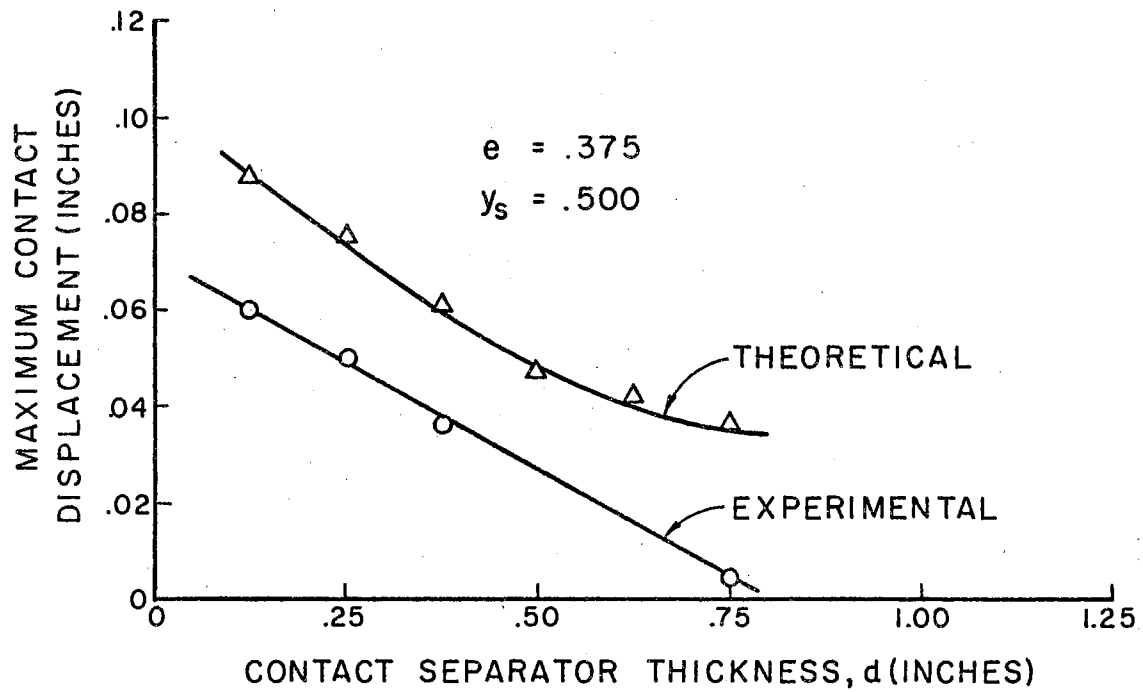


Figure 23. Theoretical and Experimental Maximum Contact Displacement

was recorded photographically. However, for each data point several experimental trials were taken in order to insure the repeatability of the data.

Several plausible explanations are possible for this discrepancy between the predictions of the hypothesized model and the experimental data from the actual model. First, the theoretically predicted impact velocities for the upper contact were never attained by the upper contact in the model. The measurements taken in the course of investigating the coefficient of restitution indicated that the experimental impact velocity was less than that predicted by theory. As indicated by the governing equation a decrease in the velocity of impact of the upper contact will decrease the magnitude of the displacement achieved by the lower contact. The diversity in the impact velocities is attributed to the release mechanism employed in the experimental model, specifically, the solenoid. The end of the solenoid plunger upon which the contact rested prior to release was round and hence precluded an instantaneous release of the upper contact. It is recommended that in future models, such as the one employed in this study, that perhaps an exploding bridge wire be employed to release the contact. In addition, the actual static deflection curve, of the upper contact, probably deviates from the deflection curve which was assumed, in Chapter III, from strength of materials theory.

A second possible reason for the occurrence of experimental displacement values which are lower than the theoretical values is that the contact buttons of the upper and lower contacts may not be exactly aligned, vertically. This would imply that the contact separator mode function should not have been evaluated at $x/L = 0.5$. Any deviation from

midspan would result in a mode function of lesser magnitude and hence a diminished initial velocity on the lower contact. This, in turn, would decrease the magnitude of the lower contact displacement.

This chapter has included a description of the experimental investigation of the natural frequencies of the contacts and the contact separator. The theoretical and experimental frequencies were compared and found to be in excellent agreement for the contacts. However, for the contact separator the values were in poor agreement, and the discrepancy was attributed to a combination of a deviation in boundary conditions, shear and rotatory inertia effects. The coefficient of restitution was studied experimentally, and it exhibited a slight decrease in magnitude as the impact velocity and contact separator thickness were increased. Finally, the experimental and theoretical values for the maximum contact separation were compared. The trends indicated by the theory and experimental data were in good agreement. The theoretical separation values were greater than the experimental values, and several causes for this discrepancy were discussed.

CHAPTER VII

CONCLUSIONS AND RECOMMENDATIONS

The subsequent conclusions have been attained as a consequence of this study.

1. The severity of any circuit discontinuity, for the contact configuration analyzed, may be determined by the prediction of the displacement response of the lower contact.

2. The magnitude of the displacement response is directly proportional to the initial static displacement and hence the impact velocity of the upper contact.

3. The coefficient of restitution is a measure of the efficiency of the impact of the upper contact on the contact separator and therefore directly influences the degree of separation of the lower contact. The magnitude of the coefficient should be minimized to reduce the contact separation.

4. The coefficient of restitution, for the specific configuration studied, was found to be a function of both the impact velocity and the contact separator thickness.

5. The magnitude of the lower contact displacement decreases, for a given initial static displacement of the upper contact, with increasing contact separator thickness.

6. For the symmetric contact configuration, the contact separator should be as massive as feasible relative to the contacts.

7. The normal mode functions, though completely determined for a given beam configuration, does present a means of minimizing the displacement response of the lower contact. A reduction in the magnitude of the displacement of the lower contact may be attained by moving the point of contiguity, between the lower contact and the contact separator, from the free end of the contact to a location closer to the clamped end.

8. The complexity of the displacement response is influenced by the point of contiguity between the contact separator and the lower contact. In general, if contact is made at the nodal point of a contact's second mode, the displacement response at that point will resemble that of a single degree of freedom system.

Recommendations for Future Analysis

In addition to the conclusions just mentioned, this study precipitated some ramifications of the problem which are recommended for additional analysis and scrutiny.

Specifically, the following areas are recommended for extended study.

1. The conclusions stated concerning the coefficient of restitution are based on the particular contact configuration used in this study. It would be fruitful if additional effort, of necessity experimental, were concentrated on the parameters which determine the magnitude of this coefficient. It would appear that there is a possibility that perhaps a contact button, other than the hemispherical shape, would be advantageous from an impact standpoint.

2. The influence of the normal mode function should be investigated more extensively. Included in such an investigation should be an inquiry into the possibility of altering the mode shapes either by a change in the beam geometry or by intentionally deviating from the ideal boundary conditions, i.e., elastic or damped supports.

3. Determination of any advantage to displacing, along the longitudinal axis of the contact separator, the points at which the contacts are contiguous with the contact separator.

4. The effect of varying material properties, such as modulus of elasticity, density and hardness of the contact buttons and contact separator on the displacement response of the lower contact.

BIBLIOGRAPHY

1. Holm, R., Electrical Contacts, Uppsala: Almqvist and Wiksells.
2. Llewellyn-Jones, F., The Physics of Electrical Contacts, Oxford: at the Clarendon Press, 1957.
3. Yonekawa, M., K. Motizuki, Review of the Damping of a System with a Friction Spring, Electrical Communication Laboratory, Nippon Telegraph and Telephone Public Corporation.
4. Russell, M. N. and S. Klein, "Vibration of Electric Contacts," Transactions of American Institute of Electrical Engineers, Vol. 63, April, 1944.
5. Wood, F. W., "Design and Selection of Miniature Sliding Contacts," Electrical Manufacturing, May, 1958.
6. Schmidt, J., "Practical Approaches to Vibration Resistant Relay Design," Proceedings, Annual National Relay Conference 1956.
7. Morris, G. E., "Methods of Studying Contact Bounce," Proceedings, Annual National Relay Conference 1957.
8. Shaw, N. C., "Contact Bounce Control," Proceedings, Annual National Relay Conference 1962.
9. Kennedy, K. K., "Relay Vibration Studies," Bell Laboratories Record, April, 1953.
10. Mindlin, R. D., and L. E. Goodman, "Beam Vibrations with Time-Dependent Boundary Conditions," Journal of Applied Mechanics, Transactions of American Society of Mechanical Engineers, Vol. 72, 1950.
11. Nothmann, G. A., "Vibration of a Cantilever Beam with Prescribed End Motion," Journal of Applied Mechanics, Transactions of American Society of Mechanical Engineers, Vol. 70, 1948.
12. Peek, R. L., Jr. and H. N. Wagar, Switching Relay Design, D. Van Nostrand Co., Inc., New York, 1955.
13. Peek, R. L., Jr. and H. N. Wagar, "Flexural Vibrations of a Propped Cantilever," Bell System Technical Journal, May, 1963.

14. Lowery, R. L., B. C. Riddle, and G. C. Stone, "Vibration Control in Relay Design," Proceedings, 11th Annual National Relay Conference 1963, Oklahoma State University, Stillwater.
15. Burkhart, M. C., "Separation Criteria of a Nonlinear Contact System in a Steady State Sinusoidal Vibration Environment," Doctor of Philosophy thesis, Oklahoma State University, Stillwater, 1965.
16. Baker, A. F., "Contact Chatter Characteristics of a Linear Viscous Damped Contact System," Doctor of Philosophy thesis, Oklahoma State University, Stillwater, 1966.
17. Pandeile, J. and M. Tacnet, "Study about Impacts and Damping Problems in a Fast Miniature Telegraph Relay," CSF (Compagnie Generale de Telegraphic Sans Fil), Paris, France, NASA-N64-19529.
18. Wikell, G., "Approach to the Analysis of the Dynamic Phenomena occurring at Contact Make in a Simply Built Flexure-Operated Relay-Spring Assembly with Springs of a Simple Geometric Form," Tele, English Edition, No. 1, 1964.
19. Takei, K., "Chattering of the Simple Vibrating System," Proceedings, International Conference on Electromagnetic Relays 1963, Sendai, Japan.
20. Shinohara, T., Y. Ohki and S. Takashi, "The Transfer Reed Switch," Development Department, Telephone Engineering Division, Nippon Electric Company, Ltd., Japan.
21. Takei, K. and S. Takashi, "Theoretical Analysis of Chattering Phenomena of Switching Relays," Proceedings, International Conference on Electromagnetic Relays 1963, Sendai, Japan.
22. Simpson, J. D., "Use of the Digital Computer with the Phase-Plane Delta Method," Master of Science thesis, Oklahoma State University, Stillwater, 1963.
23. Takamura, M., Y. Shimizu and Y. Otuka, "Chatter Vibration of Switching Relay," Review of the Electrical Communication Laboratory, Nippon Telegraph and Telephone Public Corporation, Vol. 9, No. 3-4, March-April, 1961.
24. Hertz, H., "Uber die Beruhrung Fester Elasticcher Korper," Journal fur Mathematik, Bd. 92, 1882.
25. Goldsmith, W., Impact. Edward Arnold Publishers, Ltd., London, England.
26. Kolsky, H., Stress Waves in Solids, Dover Publications, Inc., New York, New York.

27. Love, A. E. H., The Mathematical Theory of Elasticity, Cambridge University Press, London, England.
28. Timoshenko, S., Theory of Elasticity, McGraw-Hill, New York.
29. Ripperger, E. A., "Longitudinal Impact of Cylindrical Bars," Proceedings, Society for Experimental Stress Analysis, Vol. X, No. 1, 1952.
30. Davidson, T. and J. H. Meier, "Impact on Prismatical Bars," Proceedings, Society of Experimental Stress Analysis, Vol. IV, No. 1.
31. Donnell, T. H., "Longitudinal Wave Transmission and Impact," Transaction of the American Society of Mechanical Engineers, Vol. 52, No. 22, September-December, 1930.
32. Cunningham, D. M. and W. Goldsmith, "Short-Time Impulses Produced by Longitudinal Impact," Proceedings, Society for Experimental Stress Analysis, Vol. XVI, No. 2, 1959.
33. Morse, R. W., "The Velocity of Compressional Waves in Rods of Rectangular Cross Section," Journal of Acoustical Society of America, Vol. 22, No. 2, March, 1950.
34. Broberg, K. B., "Shock Waves in Elastic and Elastic-Plastic Media," Kungl. Tekniska Hogskolan, Avhandling, Stockholm, 1956.
35. Timoshenko, S. and D. H. Young, Vibration Problems in Engineering, D. Van Nostrand, Co., Inc., New York, New York, Third Edition, 1955.
36. Jacobsen, L. S. and R. S. Ayre, Engineering Vibrations, McGraw-Hill Co., Inc., New York, 1958.
37. Young, D., R. P. Felgar, Jr., "Tables of Characteristic Functions Representing Normal Modes of Vibration of a Beam," Engineering Research Series, No. 44, Bureau of Engineering Research, University of Texas, Austin, 1949.
38. Saint Venant, Barre, "de Theorie de l'elasticite' des Corps Solide de Clebsch," Paris, France, 1883.
39. Timoshenko, S., "Zur Frage nach der Wirkung eines Stosses auf einer Balken," Zeitschrift fur Mathematik und Physik, Vol. 62, 1913.
40. Lord Rayleigh, "On the Production of Vibrations by Forces of Relatively Long Duration, with Application to the Theory of Collisions," Philosophical Magazine, Series 6, Vol. 11, 1906.
41. Hertz, H., Gesammelte Werke, Leipzig, Vol. 1, 1895.

42. Lee, E. H., "The Impact of a Mass Striking a Beam," Journal of Applied Mechanics, Transactions of the American Society of Mechanical Engineers, Vol. 62, 1940.
43. Hoppmann, W. H., "Impact of a Mass on a Damped Elastically Supported Beam," Journal of Applied Mechanics, Transactions of the American Society of Mechanical Engineers, Vol. 70, 1943.
44. Dengler, M. A. and M. Goland, "Transverse Impact of Long Beams, Including Rotatory Inertia and Shear Effects," Proceedings of the First United States National Congress of Applied Mechanics, 1952.
45. Eringen, A. C., "Transverse Impact on Beams and Plates," Journal of Applied Mechanics, Transactions of the American Society of Mechanical Engineers, Vol. 75, 1953.
46. Boley, B. A., "An Approximate Theory of Lateral Impact on Beams," Journal of Applied Mechanics, Transactions of the American Society of Mechanical Engineers, Vol. 76, 1954.
47. Boley, B. A. and C. C. Chao, "Some Solutions of the Timoshenko Beam Equations," Journal of Applied Mechanics, Transactions of the American Society of Mechanical Engineers, Vol. 77, 1955.
48. Boley, B. A. and C. C. Chao, "An Approximate Analysis of Timoshenko Beams under Dynamic Loads," Transactions of the American Society of Mechanical Engineers, Vol. 78, 1956.
49. Goldsmith, G. and D. M. Cunningham, "Kinematic Phenomena Observed during the Oblique Impact of a Sphere on a Beam," Journal of Applied Mechanics, Transactions of the American Society of Mechanical Engineers, Vol. 78, 1956.

APPENDIX A

RESPONSE OF A CANTILEVER BEAM TO
INITIAL DISPLACEMENT START

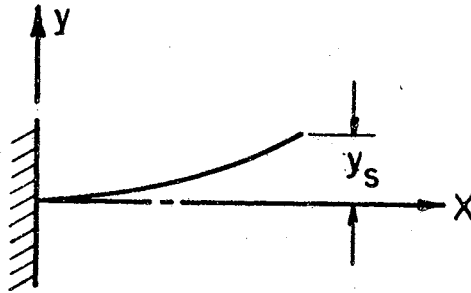


Figure 24. Cantilever Beam With An Initial Displacement

Initial Conditions:

$$y(x,0) = \frac{3y_s}{L^3} \left(\frac{Lx^2}{2} - \frac{x^3}{6} \right)$$

$$y(L,0) = y_s$$

$$\dot{y}(x,0) = 0$$

Boundary Conditions:

$$X(0) = 0; \quad X''(L) = 0$$

$$X'(0) = 0; \quad X'''(L) = 0$$

The beam is assumed to be a linear, undamped, elastic member. The transverse vibrations are restricted to the x-y plane and governed by the partial differential equation, the Euler beam equation,

$$a^2 \frac{\partial^4 y}{\partial x^4} + \frac{\partial^2 y}{\partial t^2} = 0, \quad (1)$$

where

$$a^2 = EIg/A\gamma; \quad k^2 = p/a.$$

The solution of equation (1) is a function of two variables and is assumed to have a separable form capable of being written as,

$$y(x,t) = X(x) \varphi(t). \quad (2)$$

Substitution of the above solution into (1) results in an equation permitting separation of variables and individual solutions for $X(x)$ and $\varphi(t)$ which are of the following form,

$$\begin{aligned} X(x) = & C_1 (\cos kx + \cosh kx) + C_2 (\cos kx - \cosh kx) \\ & C_3 (\sin kx + \sinh kx) + C_4 (\sin kx - \sinh kx), \end{aligned} \quad (3)$$

$$\varphi(t) = A \cos pt + B \sin pt.$$

The constants, C_i , in $X(x)$ may be evaluated by substituting the boundary conditions into the equation for $X(x)$. This results in the standard mode function and frequency equation for a cantilever beam, namely,

$$X_j(x) = C_1 (\cos k_j x - \cosh k_j x) + C_4 (\sin k_j x - \sinh k_j x) \quad (4)$$

$$\cosh k_j L \cos k_j L = -1. \quad (5)$$

The subscripts j result from the eigenvalue problem in solving the transcendental frequency equation (5) and thus necessitates the addition of the subscript in $\phi(t)$ and a summation convention over the index, j . The response equation may now be written as,

$$y(x,t) = \sum_{j=1}^{\infty} X_j(x) (A_j \cos p_j t + B_j \sin p_j t) \quad (6)$$

The constants A_j and B_j are determined solely from the starting conditions. Therefore, from the initial displacement condition

$$y(x,0) = \sum_{j=1}^{\infty} A_j X_j(x) = \frac{3y_s}{L^3} \left(\frac{Lx^2}{2} - \frac{x^3}{6} \right)$$

multiplication of both sides by $X_i(x)$ and integrating from zero to L yields,

$$\begin{aligned} \int_0^L y(x,0) X_i(x) dx &= \int_0^L \sum_{j=1}^{\infty} A_j X_j(x) X_i(x) dx \\ &= \sum_{j=1}^{\infty} A_j \int_0^L X_j(x) X_i(x) dx. \end{aligned}$$

The orthogonality condition on the mode functions dictates that

$$\int_0^L X_j(x) X_i(x) dx = L \delta_{ij} = \begin{cases} 0, & i \neq j \\ L, & i = j \end{cases}$$

and hence the integral has non-zero value at only a single index thereby precluding the summation operation. The resulting equation is therefore,

$$A_j = \frac{1}{L} \int_0^L y(x,0) X_j(x) dx \quad (7)$$

The initial conditions on velocity dictate that,

$$\dot{y}(x,0) = \sum_{j=1}^{\infty} p_j B_j X_j = 0, \text{ or}$$

$$\int_0^L \dot{y}(x,0) X_i(x) dx = \sum_{j=1}^{\infty} p_j B_j \int_0^L X_j(x) X_i(x) dx = 0.$$

The preceding equation can be reduced to,

$$p_j B_j = 0,$$

which implies that $B_j = 0$.

The displacement and velocity subsequent to the release from y_s are

$$y(x,t) = \sum_{j=1}^{\infty} A_j X_j(x) \cos p_j t, \text{ and}$$

$$\dot{y}(x,t) = \sum_{j=1}^{\infty} -p_j A_j X_j(x) \sin p_j t,$$

where A_j is defined by equation (7) and the values of $X_j(x)$ are tabulated [37].

APPENDIX B

RESPONSE OF A CANTILEVER BEAM TO AN IMPULSE AT ITS FREE END

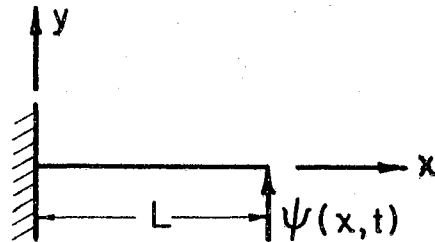


Figure 25. Transverse Impulse to the Free End
of a Cantilever Beam

$$\psi(x,t) = \psi \delta(t) \quad (1)$$

The initial conditions are assumed to be zero while the boundary condition are like those in Appendix A; however, the beam equation must contain the impulsive forcing function, $\psi(x,t)$, i.e.,

$$a^2 \frac{\partial^4 y}{\partial x^4} + \frac{\partial^2 y}{\partial t^2} = \psi(x,t) = \psi \delta(t). \quad (2)$$

Laplace transformation and virtual work techniques will be employed in determining the solution of equation (2) and the transformed variables will be denoted by capital letters, in other words,

$$Y(x,s) = \int_0^{\infty} y(x,t) e^{-st} dt.$$

The solution $y(x,t)$ is assumed to be capable of approximation by the series,

$$y(x,t) = \sum_{j=1}^{\infty} X_j(x) \varphi_j(t). \quad (3)$$

Subject to the assumption of a virtual displacement, $\delta y = X_j \delta \varphi_j$, the virtual work in the system may be written as follows:

Inertial Virtual Work, IVW

$$m\ddot{y} = m \sum_{j=1}^{\infty} X_j(x) \ddot{\varphi}_j = \frac{\gamma A}{g} \sum_{j=1}^{\infty} X_j(x) \ddot{\varphi}_j$$

$$\begin{aligned} \text{IVW} &= - \int_0^L m\ddot{y} \delta y dx = \frac{\gamma A}{g} \int_0^L \left(\sum_{j=1}^{\infty} \ddot{\varphi}_j X_j(x) \right) \delta \varphi_j X_j(x) dx \\ &= - \frac{\gamma A}{g} \ddot{\varphi}_j \delta \varphi_j \int_0^L X_j^2(x) dx \\ &= - \frac{\gamma A L}{g} \ddot{\varphi}_j \delta \varphi_j \end{aligned} \quad (4)$$

Elastic Virtual Work, EVW

$$\begin{aligned} \text{EVW} &= - \frac{EI}{2} \int_0^L \left(\frac{d^2 y}{dx^2} \right)^2 dx \\ &= - \frac{EI}{2} \int_0^L \left\{ \frac{d^2}{dx^2} \left[\sum_{j=1}^{\infty} \varphi_j X_j(x) \right] \right\}^2 dx \end{aligned}$$

$$\begin{aligned}
&= -\frac{EI}{2} \sum_{j=1}^{\infty} \varphi_j^2 \int_0^L \left[\frac{d^2 X_j(x)}{dx^2} \right]^2 dx \\
&= -\frac{EIL}{2} \sum_{j=1}^{\infty} k_j^4 \varphi_j^2
\end{aligned}$$

The virtual strain energy is therefore,

$$\begin{aligned}
EVW &= -\frac{EI}{2} \sum_{j=1}^{\infty} k_j^4 L \delta(\varphi_j^2) \\
&= -\frac{EI}{L^3} \sum (k_j L)^4 \varphi_j \delta \varphi_j.
\end{aligned} \tag{5}$$

Virtual Work from Force, FW

$$FW = \psi(t) \delta \varphi_j X_j(L) \tag{6}$$

The total virtual work is summed and equated to zero. After a rearrangement of the necessary terms from (4), (5) and (6) the resulting equation may be written as,

$$\ddot{\varphi}_j + a^2 k_j^4 \varphi_j = \frac{g\psi}{\sqrt{AL}} X_j(L) \delta(t). \tag{7}$$

The Laplace transform of (7) yields

$$s^2 \bar{\varphi}_j(s) - s \varphi_j(0) - \dot{\varphi}_j(0) + a^2 k_j^4 \bar{\varphi}_j(s) = \frac{gX_j(L)}{\sqrt{AL}} \psi \tag{8}$$

Since the initial conditions were set equal to zero,

$$\varphi(0) = 0; \dot{\varphi}(0) = 0,$$

and equation (8) may be solved for $\bar{\phi}_j(s)$ yielding

$$\bar{\phi}_j(s) = \frac{gX_j(L)}{\sqrt{AL}} \frac{\psi}{s^2 + a^2 k_j^4}.$$

The inverse transform of $\bar{\phi}_j(s)$ is,

$$\phi_j(t) = \frac{gX_j(L)}{\sqrt{AL}} \frac{\psi}{ak_j^2} \text{Sin } ak_j^2 t$$

but $ak_j^2 = p_j$ and $g/\sqrt{AL} = 1/M$, so that

$$\phi_j(t) = \frac{\psi}{M} \frac{X_j(L)}{p_j} \text{Sin } p_j t. \quad (9)$$

The substitution of (9) into (3) yields the equation for the displacement response of the beam,

$$y(x,t) = \frac{\psi}{M} \sum_{j=1}^{\infty} \frac{X_j(L) X_j(x)}{p_j} \text{Sin } p_j t. \quad (10)$$

The corresponding velocity response is therefore,

$$\dot{y}(x,t) = \frac{\psi}{M} \sum_{j=1}^{\infty} X_j(L) X_j(x) \text{Cos } p_j t. \quad (11)$$

APPENDIX C

RESPONSE OF A CLAMPED-CLAMPED BEAM TO AN
IMPULSE AT MID-SPAN

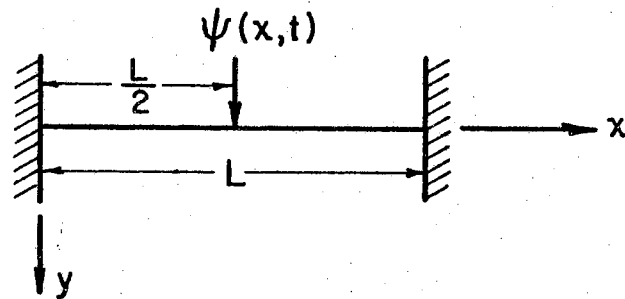


Figure 26. Transverse Impulse to a Clamped-Clamped Beam at Mid-Span

$$\psi = \psi(x, t) = \psi \delta(t) \delta(x - L/2)$$

The separator is assumed to be a linear, undamped, elastic, clamped-clamped beam with zero initial conditions which obeys the Euler beam equation,

$$a^2 \frac{\partial^4 y}{\partial x^4} + \frac{\partial^2 y}{\partial t^2} = \psi(x, t), \quad (1)$$

with a solution of the separable form, $y(x, t) = X(x) \varphi(t)$.

The boundary conditions resulting from the clamped-clamped assumption are

$$\begin{aligned} X(0) &= X(L) = 0, \\ X'(0) &= X'(L) = 0. \end{aligned} \quad (2)$$

Substitution of the boundary condition then yields the frequency equation

$$\cos k_j L \cosh k_j L = 1 \quad (3)$$

and the mode function,

$$X_j(x) = (\cosh k_j x - \cos k_j x) - \alpha_j (\sinh k_j x - \sin k_j x) \quad (4)$$

The normal mode functions are orthogonal functions and the orthogonality condition will be given by

$$\int_0^L X_j(x) X_i(x) dx = L \delta_{ij} \quad (5)$$

The function $\varphi_j(x)$ may be determined by assuming a virtual displacement, $\delta y = \delta \varphi_j X_j$, and obtaining expressions for the virtual work as in Appendix B.

The differential equation may be written as,

$$\ddot{\varphi}_j + a^2 \frac{(k_j L)^4}{L^4} \varphi_j = \frac{\psi g}{\sqrt{AL}} \delta(t) X_j(L/2).$$

The application of Laplace transforms yields the following expression for $\varphi(t)$,

$$\varphi(t) = \frac{\psi g}{\sqrt{AL}} \frac{X_j(L/2)}{p_j} \sin p_j t.$$

The complete displacement response is therefore obtained by substitution into

$$y(x, t) = \sum_{j=1}^{\infty} X_j(x) \varphi_j(t)$$

or

$$y(x,t) = \frac{\psi g}{\sqrt{AL}} \sum_{j=1}^{\infty} \frac{X_j(L/2) X_j(x)}{p_j} \sin p_j t.$$

The velocity response is,

$$\dot{y}(x,t) = \frac{\psi}{M} \sum_{j=1}^{\infty} X_j(L/2) X_j(x) \cos p_j t.$$

APPENDIX D

RESPONSE OF A CANTILEVER BEAM TO AN INITIAL
VELOCITY START AT ITS FREE END

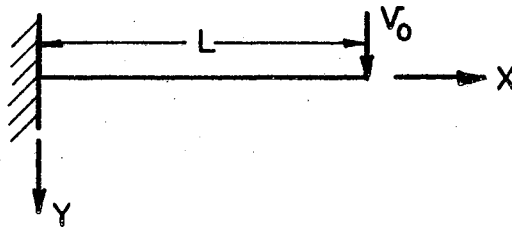


Figure 27. Initial Velocity Start to
a Cantilever Beam

Initial Conditions:

$$y(x,0) = 0$$

$$\dot{y}(x,0) = v_0 \delta(x-L)$$

The beam equation has the form,

$$a^2 \frac{\partial^4 y}{\partial x^4} + \frac{\partial^2 y}{\partial t^2} = 0 \quad (1)$$

with a solution,

$$y(x,t) = \sum_{j=1}^{\infty} X_j(x) (A_j \cos p_j t + B_j \sin p_j t). \quad (2)$$

Substitution of the initial condition on displacement into equation (2) yields,

$$y(x,0) = \sum_{j=1}^{\infty} X_j(x) A_j = 0,$$

which implies $A_j = 0$.

The initial condition on velocity yields,

$$\dot{y}(x,0) = \sum_{j=1}^{\infty} p_j X_j(x) B_j = v_0 \delta(x-L). \quad (3)$$

If both sides of (3) are multiplied by $X_i(x)$ and integrated, the resulting equation is,

$$\sum_{j=1}^{\infty} p_j B_j \int_0^L X_j(x) X_i(x) dx = \int_0^L v_0 \delta(x-L) X_i(x) dx. \quad (4)$$

However, with the orthogonality condition and the fact that

$$\int_0^L v_0 \delta(x-L) X_i(x) dx = v_0 X_i(L)$$

equation (4) reduces to the following

$$p_j B_j L = v_0 X_j(L),$$

or,

$$B_j = \frac{v_0 X_j(L)}{p_j L}.$$

The displacement response is therefore,

$$y(x,t) = \sum_{j=1}^{\infty} \frac{v_0}{L} \frac{X_j(L)}{p_j} X_j(x) \sin p_j t, \quad (5)$$

and the velocity is given by

$$\dot{y}(x,t) = \sum_{j=1}^{\infty} \frac{v_0}{L} X_j(L) X_j(x) \cos p_j t. \quad (6)$$

APPENDIX E

DISPLACEMENT EQUATIONS FOR REPEATED IMPACTS OF A CANTILEVER
BEAM, AT ITS FREE END, WITH A RIGID BODY

The curve shown below will be used to facilitate the development of a notation adequate to describe the displacement of the cantilever beam for repeated collisions with a rigid body.

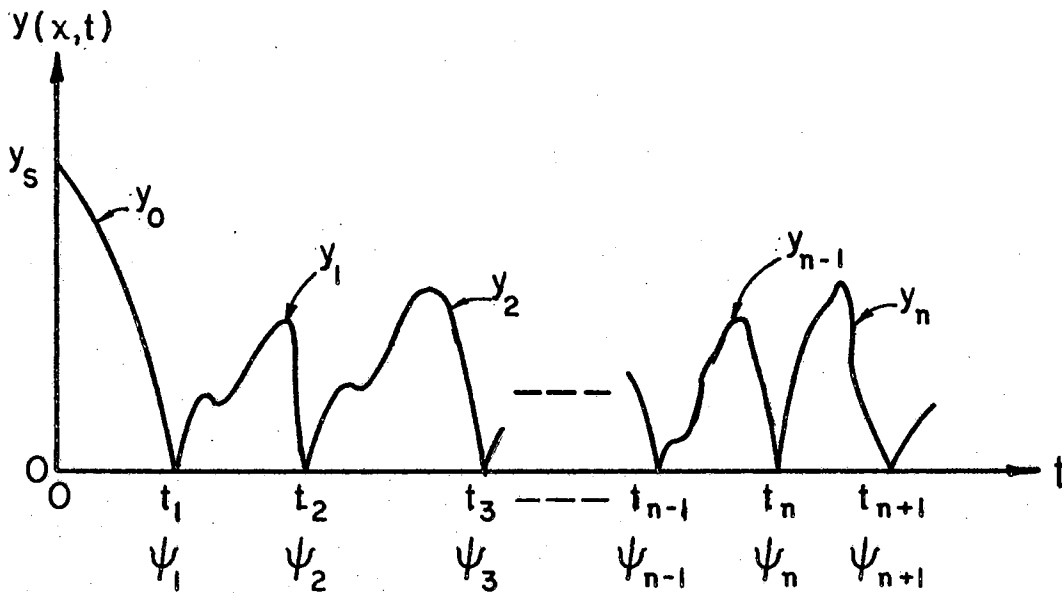


Figure 28. Contact Response During Repeated Collisions With a Rigid Body

In this figure, n is an index denoting the number of the impact, ψ_n is the impulse and y_n is the contact displacement response due to

the impact at $t = t_n$. The coefficients A_j and B_j will also have an added subscript, namely, n to associate them with a specific displacement, y_n and will be denoted as A_{jn} and B_{jn} .

For the interval $0 \leq t < t_1$, $y(x,t) = y_0(x,t)$ and is given by equations (2) and (4) of Chapter III. At $t = t_1$, the free end of the cantilever beam experiences its first impulse, ψ_1 . The coefficients A_{j1} and B_{j1} may be evaluated using boundary conditions on the contact displacement and velocity at t_1 , which may be presented as follows,

$$y_0(L, t_1^-) = y_1(L, t_1^+) = y_1(L, 0) \quad (1)$$

$$\dot{y}_1(L, 0) = \dot{y}_0(L, t_1^-) - \frac{\psi_1}{M} \sum_{j=1}^{\infty} X_j^2(L) \quad (2)$$

If the appropriate displacement equations are substituted into (1), the result is,

$$\sum_{j=1}^{\infty} A_{j0} X_j(L) \cos p_j t_1 = \sum_{j=1}^{\infty} A_{j1} X_j(L)$$

After multiplication of both sides by $X_i(x)$ and integration from $x = 0$ to $x = L$, the preceding equation may be written as,

$$\sum_{j=1}^{\infty} A_{j1} \int_0^L X_j^2(x) dx = \sum_{j=1}^{\infty} A_{j0} \cos p_j t_1 \int_0^L X_j^2(x) dx,$$

and therefore for each j ,

$$A_{j1} = A_{j0} \cos p_j t_1 \quad (3)$$

The velocity expression, equation (2), when expanded yields, for each j ,

$$B_{j1} = -A_{j0} \sin p_j t_1. \quad (4)$$

Thus, for the time interval, $t_1 \leq t, < t_2$,

$$y(x,t) = y_1(x,t) = \sum_{j=1}^{\infty} \left\{ A_{j1} \cos p_j t + \left(B_{j1} - \frac{\psi_1}{M} \frac{X_j(L)}{p_j} \right) \sin p_j t \right\} X_j(x), \quad (5)$$

where A_{j1} and B_{j1} are given by (3) and (4), respectively.

It is now possible to obtain a general recursion relation for the coefficients A_{jn} and B_{jn} in terms of $A_{j(n-1)}$ and $B_{j(n-1)}$ by using the following equations,

$$y_n(L,0) = y_{n-1}(L, t_n - t_{n-1}) \quad (6)$$

$$\dot{y}_n(L, t_n^+) = \dot{y}_{n-1}(L, t_n - t_{n-1}) - \frac{\psi_n}{M} \sum_{j=1}^{\infty} X_j^2(L).$$

Substitution into (6) yields,

$$A_{jn} = A_{j(n-1)} \cos p_j (t_n - t_{n-1}) \quad (7)$$

$$B_{jn} = -A_{j(n-1)} \sin p_j (t_n - t_{n-1})$$

$$+ \left[B_{j1} - \frac{\psi_{(n-1)}}{M} \frac{X_j(L)}{p_j} \right] \cos p_j (t_n - t_{n-1})$$

and the corresponding displacement response is

$$y_n(x,t) = \sum_{j=1}^{\infty} \left\{ A_{jn} \cos p_j t + \left(B_{jn} - \frac{\psi_n}{M} \frac{X_j(L)}{p_j} \right) \sin p_j t \right\} X_j(x) \quad (8)$$

valid for the time interval $t_n \leq t \leq t_{(n+1)}$.

The expression for the impulse may be derived using the method of Section D of Chapter III and the resulting expression is,

$$\psi_n = \frac{(1 + e)M \sum_{j=1}^{\infty} p_j B_{jn} X_j(L)}{\sum_{j=1}^{\infty} X_j^2(L)} \quad (9)$$

APPENDIX F

LIST OF MAJOR INSTRUMENTATION

- Audio Oscillator--Model 200 AB; Manufacturer, Hewlett-Packard; Serial No. 130-13888.
- Universal EPUT and Timer--Model 7360; Manufacturer, Beckman-Berkley; Serial No. 370.
- Dual Beam Cathode Ray Oscilloscope--Model 502; Manufacturer, Tektronix; Serial No. 26.
- Velocity Transducer--Model 6LV2; Manufacturer, Sanborn Company; Serial No. HH.
Model 6LV1; Serial No. HH.
- Electromechanical Shaker--Model C-10E; Manufacturer, MB Electronics; Serial No. 121.
Model C-11; Serial No. 670.
- Power Supplies (D.C.)--Programmable Regatron; Manufacturer, Electronic Associates; Serial No. 348.
Model 865B; Manufacturer, Harrison Laboratories; Serial No. 23.
- Light Sources--Model Optic-Lume Illuminators; Manufacturer, Baush & Lomb.
- Photocells--Model 10-6L; Manufacturer, Solar Systems.

APPENDIX G

FORTRAN PROGRAM FOR THE LOWER CONTACT
DISPLACEMENT

```

C   PRINTED CIRCUIT BOARD CONTACT SEPARATION ANALYSIS
    DIMENSION V(4),C(4),ALPHA(4),DOG(4),SINH(4),COSH(4),P(4),U(4),Q(4)
    DIMENSION R(4),D1(4),D2(4),D3(4),D4(4),D5(4),D6(4),D7(4),D8(4)
    DIMENSION AP(4),PE(4),A1(4),B1(4,6),APE(4)
    DIMENSION V2(4), C2(4), ALPH2(4), V3(4), C3(4), ALPH3(4)
    DIMENSION P2(4), P3(4), C2S(4), C3S(4)
10  FORMAT( 7F15.9)
15  FORMAT (E15.9,I2)
20  FORMAT (15,I5,I5,I5,I5,I5,I5)
5   READ(5,10) XL,B,H,RHO,YSTAT
    READ (5,10) XL2, B2, H2,RHO2
    READ (5,10)XL3,B3,H3,RHO3
    READ (5,10) DELT,ER,DELY
    READ (5,15) E,N
    READ (5,10) XL2C
    WRITE (6,10) XL2 ,B2, H2, RHO2
    DT = DELT
    RHOC = (RHO) / 1728.0
    RHO2C = RHO2 / 1728.0
    RHO3C = RHO3 / 1728.0
    A = B * H
    A2 = B2 *H2
    A3 = B3 * H3
    WM = (RHOC *A *XL )/386.4
    WM2 = ( RHO2C * A2*XL2) / 386.4
    WM3 = (RHO3C * A3 * XL3) / 386.4
    EYE = (B*(H **3)) / 12.0
    EYE2 = (B2*(H2**3)) / 12.0
    EYE3 = (B3*(H3**3)) / 12.0
    W=SQRT((E*(EYE*386.4))/(A*RHOC))
    W2 = SQRT((E*(EYE2 * 386.4)) / (A2* RHO2C ))
    W3 = SQRT((E* ( EYE3 * 386.4)) / (A3 * RHO3C))
30  DO 35 I = 1, N
    READ (5,10) V(I), C(I), ALPHA(I)
35  CONTINUE
36  DO 37 I = 1,N
    READ (5,10) V2(I), C2(I), ALPH2(I)
37  CONTINUE
38  DO 39 I = 1,N
    READ (5,10) V3(I), C3(I), ALPH3(I)
39  CONTINUE
60  DO 70 I=1,N
    DOG(I)=-V(I)
    SINH(I)=(EXP(V(I))-EXP(DOG(I)))/2.0
    COSH(I)=(EXP(V(I))+EXP(DOG(I)))/2.0
    P(I) = (W * (V(I) ** 2 )) / (XL **2 )
    U(I) = V(I) / XL
    Q(I)=2.0/(U(I)**3)
    R(I)=(XL**2)/U(I)
    D1(I)=(Q(I)-R(I))*COS(V(I))+((2.0*(XL*SIN(V(I))))/(U(I)**2))-Q(I)
    D2(I)=(((2.0*XL)*COS(V(I)))/(U(I)**2))+(R(I)-Q(I))*SIN(V(I))
    D3(I)=((3.0*D2(I))/U(I))-((XL**3)*COS(V(I)))/U(I)
    D4(I)=((XL**3)*SIN(V(I))/U(I))-3.0*D1(I)/U(I)
    D5(I)=(R(I)+Q(I))*COSH(I)-((2.0*XL)*SINH(I)/(U(I)**2))-Q(I)
    D6(I)=((R(I)+Q(I))*SINH(I))-((2.0*XL)*COSH(I)/(U(I)**2))
    D7(I)=((XL**3)*COSH(I)/U(I))-3.0*D6(I)/U(I)
    D8(I)=((XL**3)*SINH(I)/U(I))-3.0*D5(I)/U(I)
    AP(I)=((3.*YSTAT)/(XL**3))*((D6(I)-D2(I))-ALPHA(I)*(D5(I)-D1(I)))
    PE(I)=(YSTAT/(XL**4))*((D8(I)-D4(I))-ALPHA(I)*(D7(I)-D3(I)))
    APE(I)=(AP(I)-PE(I))/2.0
    WRITE (6,10) V(I),C(I),ALPHA(I), P(I), APE(I)
70  CONTINUE

```

```

      T=0.0
80    TY=0.0
      TYDTL=0.0
      ACT = 0.0
      CT=0.0
      CT2 = 0.0
      CT3 = 0.0
90    DO 100 I=1,N
      Y=APE(I)*C(I)*COS(P(I)*T)
      TY=TY+Y
      YDTL=-P(I)*APE(I)*C(I)*SIN(P(I)*T)
      TYDTL=TYDTL+YDTL
      AC=-P(I)*APE(I)*C(I)
      ACT=ACT+AC
      C1 = C(I) **2
      CT = CT + C1
      C2S(I) = C2(I)**2
      CT2 = CT2 + C2S(I)
      C3S(I) = C3(I) **2
      CT3 = CT3 + C3S(I)
100   CONTINUE
      IF (TY-DELY)130,131,110
110   WRITE(6,10)T, TY, TYDTL
      IF (DELT-0.0005)120,115,115
115   NT=T/(0.01/100.)
      NTY=TY/(0.1/100.)
      M=3
120   IF (DELT-0.00000001)131,131,122
122   TT=T
125   T=T+DELT
      GO TO 80
130   T=TT
      DELT=(DELT)/2.0
      T=T+DELT
      GO TO 80
131   ED=9.999
      WRITE (6,10)ED
132   EY = ((1.0 +ER) * ACT) / ((CT/WM) + (CT2/WM2) + ( CT3/WM3 ))
      WRITE(6,10) T,EY,CT,CT2,CT3
      DO 133 I=1,N
      K=I+1
      X=N
      J=1
      A1(I) = APE(I) * COS( P(I) * T)
      B1(I,J)=-APE(I)*SIN(P(I)*T)
      WRITE (6,10) A1(I) ,B1(I,J)
133   CONTINUE
170   T=0.0
200   TY=0.0
      TYDTL=0.0
      ACT=0.0
240   DO 300 I=1,N
      Y=A1(I)*COS(P(I)*T)
      Y=(Y+(B1(I,J)-((EY*C(I))/(WM*P(I))))*SIN(P(I)*T))*C(I)
      TY=TY+Y
      YDTL=-A1(I)*(SIN(P(I)*T))
      YDTL=(YDTL+(B1(I,J)-((EY*C(I))/(WM*P(I))))*COS(P(I)*T))*C(I)*P(I)
      TYDTL=TYDTL+YDTL
      AC=P(I)*B1(I,J)*C(I)
      ACT=ACT+AC
300   CONTINUE
315   WRITE (6,10)T, TY, TYDTL ,ACT

```

```
350 TY2DT = 0.0
      WM2 = WM2 * ( XL2C / XL2 )
400 DO 410 I = 1,N
      P2(I) = (W2 * (V2(I) **2)) / ( XL2 **2)
      P3(I) = (W3 * (V3(I) **2 )) / ( XL3**2 )
      Y2DT = (EY/WM2 ) * C2S(I)
      TY2DT = TY2DT + Y2DT
410 CONTINUE
      WRITE(6,10) TY2DT
450 TY3 = 0.0
500 DO 510 I = 1,N
      Y3 = TY2DT * (C3S(I) * SIN(P3(I) *T)) / (XL3 *P3(I) )
      TY3 = TY3 + Y3
510 CONTINUE
      TAU = 0.060
      WRITE (6,10) T, TY3
      DELT = DT
      T = T + DELT
      IF ( T - TAU) 520, 600, 600
520 GO TO 450
600 DO 610 I = 1,N
      WRITE(6,10) V2(I),C2(I),ALPH2(I), P2(I)
610 CONTINUE
650 DO 660 I = 1,N
      WRITE (6,10) V3(I), C3(I), ALPH3(I), P3(I)
660 CONTINUE
      GR = H2 / XL2
      BETA = WM / (WM2 + WM3)
      MR1 = WM2 / WM
      MR3 = WM2 / WM3
      WRITE (6,10) WM, WM2, WM3 ,XL2C
      WRITE(6,10) GR, BETA, MR1 ,MR3
      GO TO 5
      END
```


VITA

Heinz Walter Schmitt

Candidate for the Degree of

Doctor of Philosophy

Thesis: THE DYNAMIC ANALYSIS OF CONTACT SEPARATION DUE TO IMPACT IN A
CONTINUOUS, REDUNDANT CONTACT SYSTEM

Major Field: Mechanical Engineering

Biographical:

Personal Data: Born February 9, 1937, in New York, New York, the
son of Walter and Minnie Schmitt. Married to Barbara Diane
Hoeke on September 22, 1962. Father of a son, Karl Stephen,
born November 14, 1965.

Education: Graduated from Grover Cleveland High School, Ridgewood,
New York, 1954; received Bachelor of Mechanical Engineering
Degree from Brooklyn Polytechnic Institute in June, 1960;
received Master of Science Degree from the University of New
Mexico in June, 1962, as a participant of the Sandia Corporation
Technical Development Program; completed requirements for the
Doctor of Philosophy Degree at Oklahoma State University in
February, 1965.

Professional Experience: Draftsman, Bell Telephone Laboratories,
Inc., 1955 to 1957. Quality Control Engineer, General Electric
Company, summer of 1959. Project Engineer, Electromechanical
Switch Design and Development, Sandia Corporation, June, 1960,
to September, 1963, and June, 1964, to September, 1964. Gradu-
ate Assistant, Oklahoma State University, September, 1963, to
June, 1964, and September, 1964, to February, 1966.

Organizations: Tau Beta Pi, American Society of Mechanical Engineers,
Acoustical Society of America, Professional Engineer (Oklahoma).